NORSAR

ROYAL NORWEGIAN COUNCIL FOR SCIENTIFIC AND INDUSTRIAL RESEARCH

Scientific Report No. 3-73/74

ANALYSIS OF CODA AND MULTIPATH PROPAGATION OF RAYLEIGH WAVES AT NORSAR

by
H. Bungum and J. Capon

Kjeller, 3 January 1974

SECURITY CLASSIFICATION OF THIS PAGE *(When Data Entered)*

REPORT DOCUMENTATION PAGE

READ INSTRUCTIONS BEFORE COMPLETING FORM

1. REPORT NUMBER: F44620-74-C-0001	2. GOVT ACCESSION NO.
3. RECIPIENT'S CATALOG NUMBER	
4. TITLE *(and Subtitle)*: Analysis of Coda and Multipath Propagation of Rayleigh Waves at NORSAR	5. TYPE OF REPORT & PERIOD COVERED: Scientific Report
6. PERFORMING ORG. REPORT NUMBER: Scientific Report 3-73/74	
7. AUTHOR(s): H. Bungum and J. Capon* *M.I.T. Lincoln Lab, Seismic Discrimination Group, Cambridge, Mass., U.S.A.	8. CONTRACT OR GRANT NUMBER(s): F44620-74-C-0001
9. PERFORMING ORGANIZATION NAME AND ADDRESS: NTNF/NORSAR Post Box 51 N-2007, Kjeller, Norway	10. PROGRAM ELEMENT, PROJECT, TASK AREA & WORK UNIT NUMBERS: NORSAR Phase 3
11. CONTROLLING OFFICE NAME AND ADDRESS: Air Force Office of Scientific Research 1400 Wilson Blvd Arlington, Virginia 22209, U.S.A.	12. REPORT DATE: 3 January 1974 13. NUMBER OF PAGES: 62
14. MONITORING AGENCY NAME & ADDRESS *(if different from Controlling Office)*: European Office of Aerospace Research and Development Keysign House, 429 Oxford Street London W1, England Attn: Maj.F.D. Munzlinger	15. SECURITY CLASS. *(of this report)* 15a. DECLASSIFICATION/DOWNGRADING SCHEDULE
16. DISTRIBUTION STATEMENT *(of this Report)*: Approved for public release; distribution unlimited.	
17. DISTRIBUTION STATEMENT *(of the abstract entered in Block 20, if different from Report)*	
18. SUPPLEMENTARY NOTES	
19. KEY WORDS *(Continue on reverse side if necessary and identify by block number)*: Seismic arrays, Rayleigh waves, Seismic detection, Multipath propagation, Ray path.	

20. ABSTRACT *(Continue on reverse side if necessary and identify by block number)*

Frequency-wavenumber analysis of coda of 40 and 20 sec Rayleigh waves recorded at NORSAR shows that 40 sec period coda drops off faster vs. time while the resolving power of the array is better at 20 sec. Multipath arrivals with as much as 40°-60° are frequently identified, and travel path solutions for some events are proposed. As an example, 20 sec Rayleigh waves from a nuclear explosion are identified in the presence of an interfering event.

DD FORM 1 JAN 73 1473 EDITION OF 1 NOV 65 IS OBSOLETE

SECURITY CLASSIFICATION OF THIS PAGE *(When Data Entered)*

Scientific Report No. 3-73/74

ANALYSIS OF CODA AND MULTIPATH PROPAGATION OF RAYLEIGH WAVES AT NORSAR

by

H. Bungum* and J. Capon**

Kjeller, 13 January 1974

* NTNF/NORSAR
Kjeller, Norway

** M.I.T. Lincoln Laboratory
Seismic Discrimination Group
Cambridge, Massachusetts, USA

USAF Project Authorization No.:		VT/4702/B/OSR
Date of Contract	:	30 August 1973
Amount of Contract	:	$ 888,806.00
Contract Termination Date	:	30 June 1974
Project Supervisor	:	Robert Major, NTNF
Project Manager	:	Nils Marås
Title of Contract	:	Norwegian Seismic Array (NORSAR)

CONTENTS

ANALYSIS OF CODA AND MULTIPATH PROPAGATION OF RAYLEIGH WAVES AT NORSAR

ABSTRACT

The coda of Rayleigh waves from 15 earthquakes recorded at the Norwegian Seismic Array (NORSAR) have been analyzed in wavenumber space at periods of 40 and 20 sec. The power at 40 sec drops off faster vs. time, which reduces the probability of interference between events. On the other side, the capability of the array to resolve signals under various conditions is better at 20 sec. Since also the frequency distribution of signal power varies, one cannot determine any specific frequency as generally having the best signal-to-interference ratio. The detection problem is also complicated by considerable multipath propagation, which is most severe at 20 sec. Multipath arrivals with as much as 40°-60° azimuthal deviation are frequently identified, and a number of travel path solutions for different events are proposed. Usually the rays have been found to be refracted or reflected at continental boundaries. As an example, an atmospheric nuclear explosion from Lop Nor has been used to illustrate these various aspects of the problem of detecting one Rayleigh wave in the presence of another.

INTRODUCTION

One of the most powerful methods available today for discriminating between natural earthquakes and underground explosions is the m_b:M_s method, based on the relationship between the body wave (m_b) and the surface wave (M_s) magnitude. Considerable efforts have been invested on the problem of magnitude definitions, and especially how to find a definition of M_s yielding the best possible separation between earthquakes and explosions on an m_b:M_s diagram (cf. Marshall and Basham 1972). However, with the present deployment of seismic stations the main restriction of the method is quite often that no surface waves at all are found from an event which is detected and located on the basis of short period recordings. Besides the fact that the background noise of the

earth always is the main limiting factor, a lack of surface waves can of course be due to the event being an explosion, in which case we are into the problem of negative evidence. However, quite often there is a serious detection problem caused by the interference of other events (cf. Capon and Evernden 1971). This situation is complicated by the fact that rapid lateral variations in phase velocity frequently cause severe multipathing (cf. Capon 1970). It is the aim of the present study to investigate the amount and the characteristics of such multipathing in Rayleigh waves recorded at NORSAR, and to consider the problem of detecting one Rayleigh wave in the presence of the coda of another. The short period detection capabilities of the NORSAR array are fairly well documented (cf. Bungum and Husebye 1974), and a study using the long period data for discrimination has also been presented (Filson and Bungum 1972). In this paper, other important characteristics of the long period Rayleigh waves recorded at NORSAR will be studied in the same general context.

The physical configuration of NORSAR is shown in Fig. 1 (for a detailed presentation, see Bungum et al 1971). The long period part of the array consists of one three-component set of instruments in each of the 22 subarrays, with peak response around 25 seconds. The diameter of the array is around 110 km, and the geometry is regular enough to ensure no significant azimuthal anomalies in the array response (Fig. 2). This is important when the azimuthal anomalies of the data is one of the things to be studied.

The main analysis technique used in this paper is the high-resolution (HR) frequency-wavenumber analysis, described

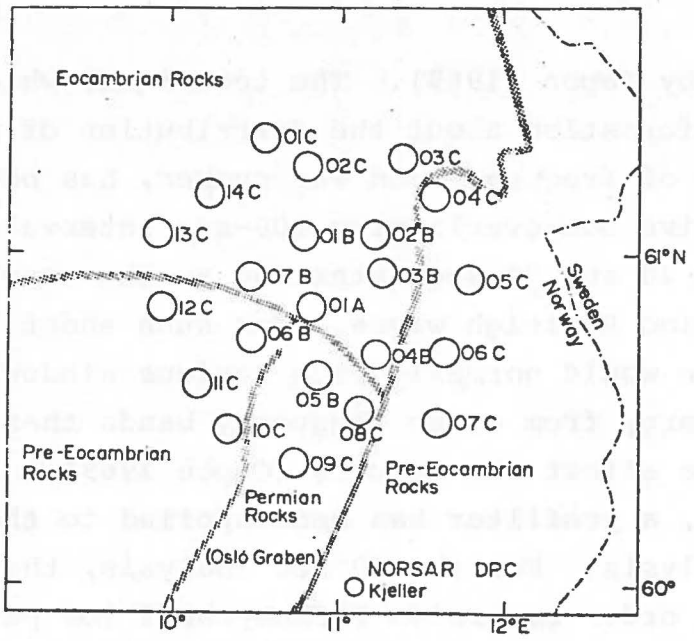

Fig. 1 NORSAR array configuration. Each circle indicates one subarray, consisting of 6 short period vertical seismometers and one three-component set of long period seismometers.

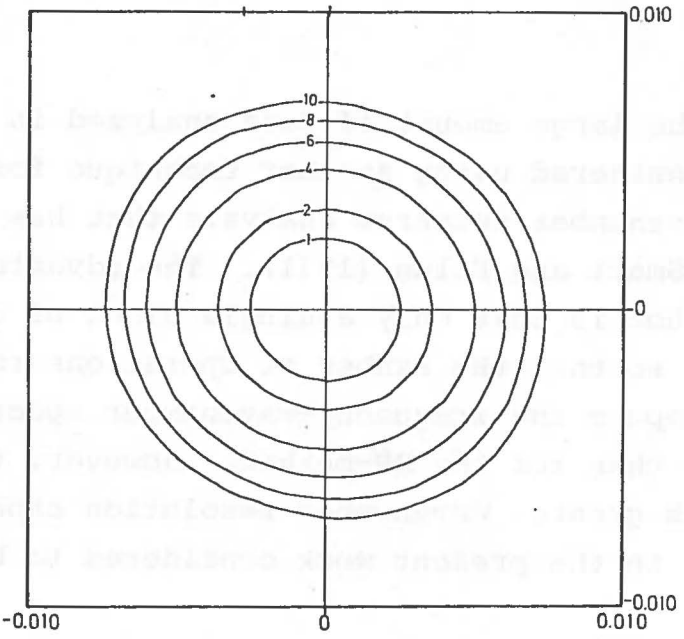

Fig. 2 Single frequency response pattern for the NORSAR long period array. The axes are in wavenumber (c/km) and the contour curves are in dB down from maximum, which also applies to all the wavenumber spectra in this paper.

in detail by Capon (1969). The technique, which essentially reveals information about the distribution of power as a function of frequency and wavenumber, has been applied to successive non-overlapping 200-sec intervals, at periods of 40 and 20 sec, starting at the onset of the 40 sec period Rayleigh waves. For such short time intervals, there would normally be a serious windowing effect, causing energy from other frequency bands than those under analysis to affect the results (Capon 1969). In order to avoid this, a prefilter has been applied to the data before the HR-analysis. For the 40 sec analysis, the filter has been a 5th order recursive Tschebycheff low pass filter with cutoff (3 dB) at 35 sec, and for the 20 sec analysis we have used a 3rd order recursive Butterworth bandpass filter with cutoffs at 25 and 16.7 sec. Both filters are rolling off very sharply, at around 35 dB/octave, thus virtually eliminating all problems connected to frequency windowing.

Because of the large amount of data analyzed in this study, we considered using another technique for frequency-wavenumber spectrum analysis that has been proposed by Smart and Flinn (1971). The advantage of their method is that only a single block of data is analyzed, so that the number of operations required to compute the frequency-wavenumber spectrum is much less than for the HR-method. However, the HR-method has greater wavenumber resolution capabilities and this was in the present work considered to be more essential.

SIMULATION OF INTERFERING EVENTS

In this paper 40 and 20 sec period Rayleigh wave codas are analyzed in successive time intervals of 200 seconds. The data are first prefiltered, then the spectral matrix is formed by averaging results from 2 blocks each of 100 seconds, whereupon the transformation to wavenumber space is done. With such a combination of short time intervals and low frequencies, where only 2.5 periods are contained in each block in the worst case, it is important to investigate carefully the stability of the results. Also, for the 40 sec analysis the diameter of the array is less than one wavelength, which gives a fairly poor beam pattern as demonstrated in Fig. 2. At 20 sec, the resolution is naturally twice as good. For all these reasons, we are obviously working close to the limits of the method. An extensive test procedure involving simulated and real events has therefore been developed, in order to determine where the limits are, and what the capabilities and the limitations of the method are.

The basic results of the simulation are given in Table 1, and the procedure has been the following. Two sine waves were generated, having the same frequency (40 or 20 sec period), the same velocity (4 km/sec) but different azimuth separations (15, 30 or 90 degrees). Another important parameter is the degree to which the two waves overlap in time. If the overlap is 100%, i.e., both sine waves occupy the same 200 sec time interval, the case is simple to evaluate analytically. It is assumed that two sine waves with the same amplitude (unity), the same frequency (f), the same velocity (v), but with different wavenumber vectors ($\underline{k}_1$ and $\underline{k}_2$), are arriving simultaneously at a station with position vector $\underline{r}$. Under these conditions, only the azimuth is different, such that

$$|\underline{k}_1| = |\underline{k}_2| = |\underline{k}| \qquad (1)$$

The two waves will then be

$$X_1(t) = \exp[2\pi i(ft - \underline{k}_1 \cdot \underline{r})] \qquad (2)$$

and

$$X_2(t) = \exp[2\pi i(ft - \underline{k}_2 \cdot \underline{r})] \qquad (3)$$

TABLE 1

The quality of the wavenumber separation using the HR-method on simulated sine waves with different wavenumber distance and overlap in time. T is signal period (sec), $\Delta\alpha$ is azimuth separation (degrees) and Δk is the wavenumber distance (c/km) between the two input sine waves. The column labeled (a)-(d) refers to the wavenumber spectra in Fig. 3.

T (sec)	40	20 (40)	20	40	20
$\Delta\alpha$ (deg)	15	15 (30)	30	90	90
$\Delta k \cdot 10^3$ (c/km)	0.8	1.6	3.2	4.4	8.8
No overlap	No	Poor	Fair	Good (a)	Good
25% overlap	No	No	Poor	Fair (b)	Good
50% overlap	No	No	No	Poor (c)	Good
Full overlap	No	No	No	No (d)	No

and the sum of the two can be shown to be

$$X(t) = X_1(t) + X_2(t)$$

$$= 2 \cos[2\pi(\frac{\underline{k}_1-\underline{k}_2}{2} \cdot \underline{r})] \exp[2\pi i(ft - \frac{\underline{k}_1+\underline{k}_2}{2} \cdot \underline{r}] \quad (4)$$

This is a new sine wave with the same frequency (f) as in (2) and (3), and with a wavenumber which, following (1), will be

$$\left|\frac{\underline{k}_1+\underline{k}_2}{2}\right| \leq |\underline{k}| \quad (5)$$

with equality only for the trival case

$$\underline{k}_1 = \underline{k}_2 \quad (6)$$

In other words, this means that the sum of the two sine waves will be a new sine wave with azimuth between the two and with a smaller wavenumber, i.e., higher velocity.

The results obtained above are of great importance in this study, since they show that a high observed velocity may be erroneous, caused by the superposition of two waves with normal velocities. This has made it necessary in the interpretations of the data to impose certain restrictions on what phase velocities to accept, as discussed below. Also, for the same reason the amount of time overlap was used as an input parameter in the simulation results presented in Table 1, where the other essential entry is wavenumber difference. The table shows that the minimum azimuthal separation for which one in

practice can expect to obtain a reasonable separation is about 30^{o} (this is not the precision with which a single wave can be determined, see Appendix). Also, one can see that with as much as 50% overlap between waves, sufficient resolution is obtained only for quite large wavenumber differences. In order to demonstrate what these simulation results look like in wavenumber space, and what the designations good/fair/poor/no mean to the authors, one column in Table 1 ($\Delta k = 4.4 \cdot 10^{-3}$ c/km) has been displayed in Fig. 3. Note especially, with reference to equation (4), the result for full overlap of the sine waves: a sharp peak is found right between the two input azimuths, and the velocity has increased from 4.0 to 5.9 km/sec (Fig. 3d).

Another simulation experiment was done where the purpose was to investigate the detectability of a multipath arrival in the presence of the main group, or vice versa. Two real events were used this time, event 4 and 14 in Table 2, and 200 sec of the main 40 sec group arrival were selected for each event, as shown in Fig. 4. The experiment involved adding the two events together, with different scaling, and then passing the sum through an HR analysis. Note that the time intervals chosen are such as to give a favourable overlap between the arriving groups. The main results are given in Fig. 5 (a-d) where event 4 (North Atlantic Ridge) is scaled down 10 dB at a time relative to event 14 (Hindu Kush). In Fig. 5a event 4 is around 17 dB above event 14, which is on the limit of being detected. After being scaled down 30 dB, event 4 is still clearly detected in Fig. 5d, the power now being 8-10 dB below that of event 14. In this example, therefore, one can conclude that a multipath arrival can still be detected at a power level 12-15 dB below that of the main arrival when both occur in the

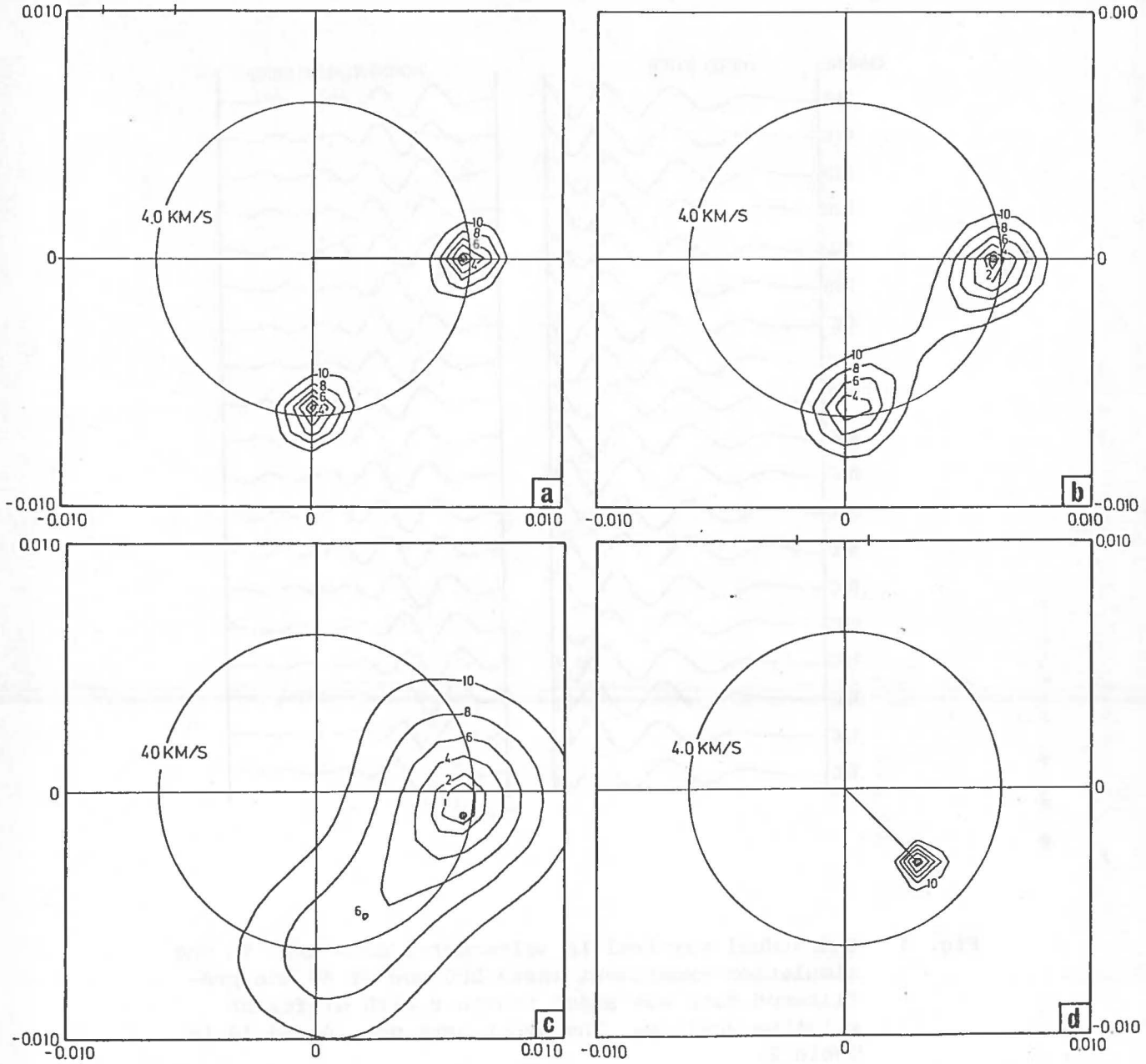

Fig. 3 Wavenumber spectra for simulation data using the HR-method on the sum of two sine waves 90° apart, but with different degree of overlap in time. The four spectra (a-d) are the same as those considered in the fourth column of Table 1. Each spectrum is estimated from two 100 sec blocks of data.

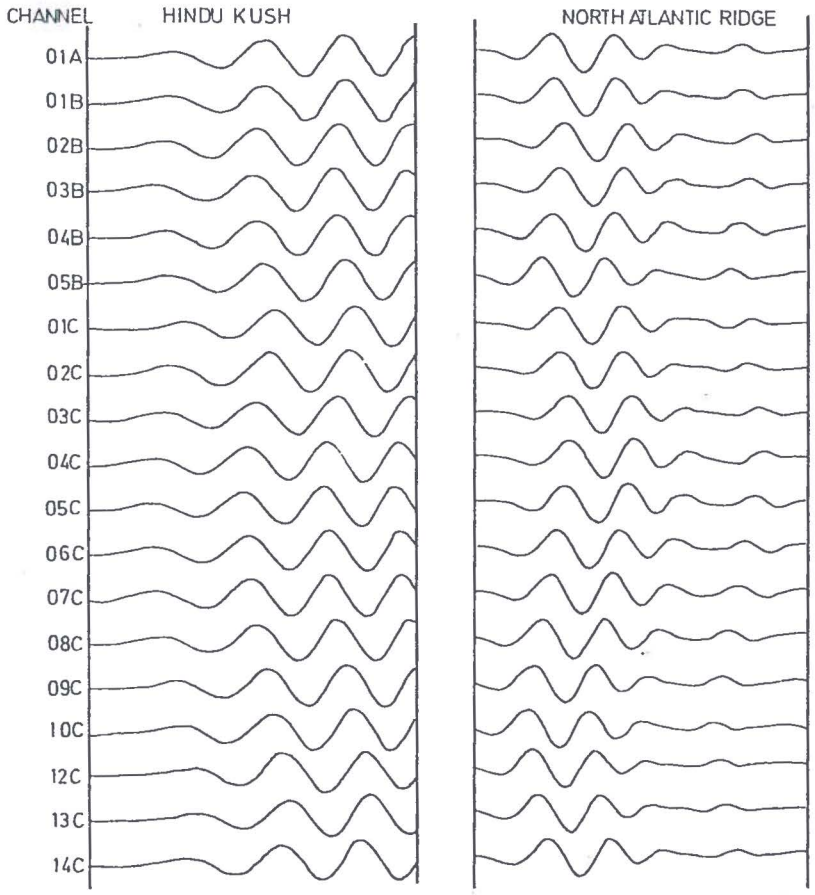

Fig. 4 Individual vertical LP seismometer data used in the simulation experiment where 200 sec of 40 sec pre-filtered data was added together with different relative scaling. The events are nos. 4 and 14 in Table 2.

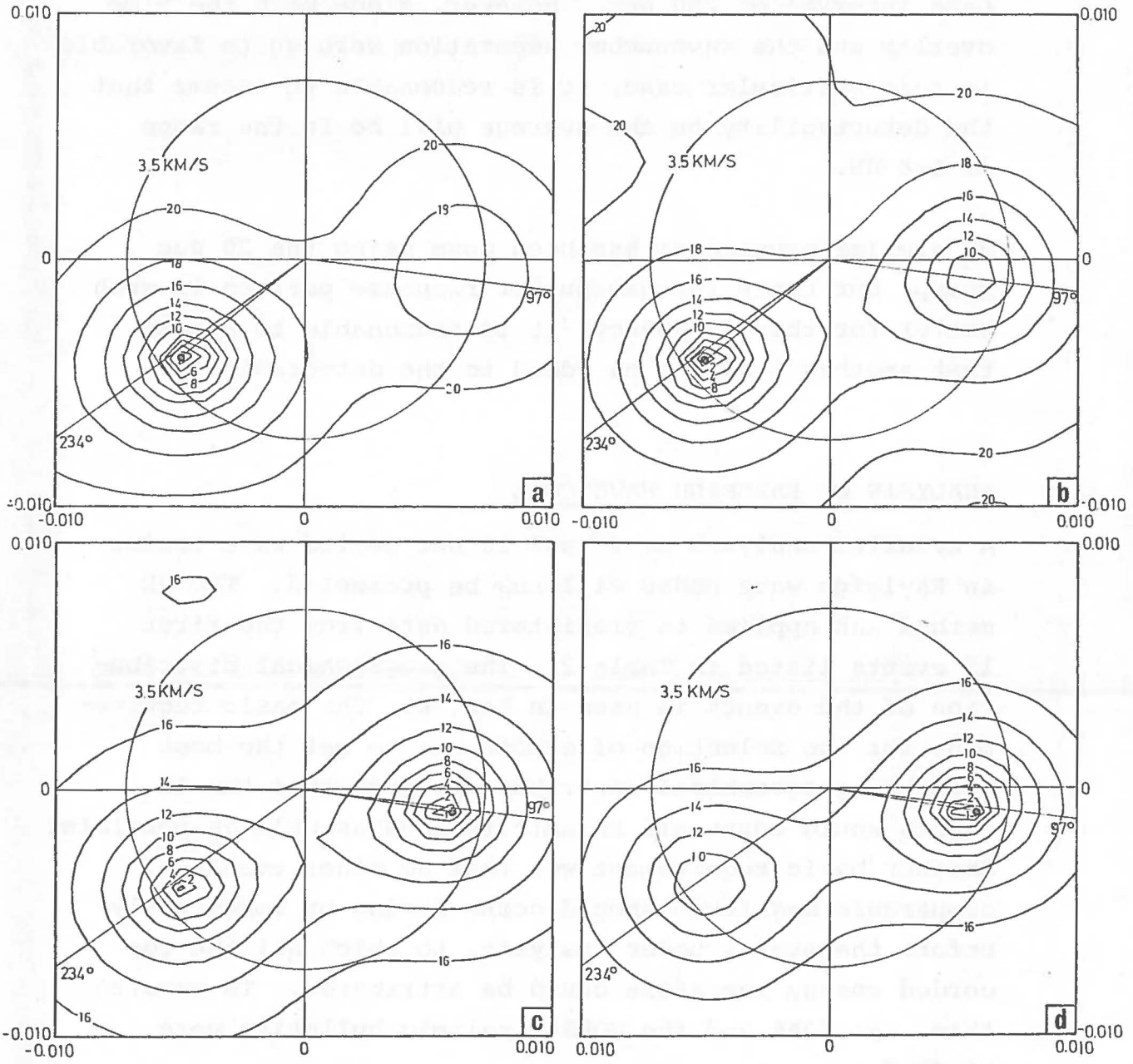

Fig. 5 Wavenumber spectra for 40 sec period simulation data using the HR-method on the sum of the two events displayed in Fig. 4. The event from North Atlantic Ridge (no. 4) is scaled down 10 dB at a time relative to the Hindu Kush event (no. 14). The true azimuths to the two events are indicated (234° and 97°).

same interval of 200 sec. However, since both the time overlap and the wavenumber separation were quite favorable in this particular case, it is reasonable to assume that the detectability on the average will be in the range of 6-8 dB.

No similar experiment has been done using the 20 sec group, but since the wavenumber response pattern is much better for this frequency, it is reasonable to assume that another 6 dB can be added to the detectability.

ANALYSIS OF RAYLEIGH WAVE CODA

A detailed analysis of 40 and 20 sec period wave trains in Rayleigh wave codas will now be presented. The HR method was applied to prefiltered data from the first 15 events listed in Table 2. The geographical distribution of the events is seen in Fig. 6. The basic requirement for the selection of events was to get the best possible geographical distribution, such that the 15 events would cover all seismic regions as well as possible. Another basic requirement was that no other events of comparable magnitude should occur during or immediately before the events under analysis, to which all the recorded energy therefore could be attributed. To ensure this, the NOAA and the NORSAR seismic bulletins were studied.

A representative example of the data under analysis is presented in Fig. 7, showing the unfiltered data, together with the 40 and 20 sec prefiltered data for event 1 (Bouvet Islands). The data panels in Fig. 7 show the main reason why we are working with the 40 sec period waves; the power at that frequency falls off more rapidly than at 20 sec, since it requires larger discontinuities to diffract the longer wavelengths (Capon 1970).

No.	Date	Origin Time (H M S)	Latitude (Deg)	Longitude (Deg)	Depth (km)	m_b	Region	Distance (Deg)	Azimuth (Deg)
1	07 Dec 71	03.26.19.9	54.4S	5.9E	33	5.7	Bouvet Islands	115	183
2	07 Feb 72	19.14.47.6	8.5N	83.9W	14	5.5	Costa Rica	85	279
3	19 Mar 72	15.57.50.4	40.8N	141.9E	76	6.0	Honshu, Japan	71	37
4	06 Jun 72	05.25.50.2	32.9N	39.9E	33	5.5	North Atlantic Ridge	43	253
5	12 Jun 72	19.47.37.2	53.3N	166.8W	44	5.8	Fox Islands	66	359
6	05 Jul 72	10.16.38.4	49.5N	127.2W	27	5.8	Vancouver Island	65	331
7	22 Jul 72	16.41.04.0	31.4N	91.5W	33	5.5	Tibet	59	81
8	12 Aug 72	09.42.05.2	51.4N	179.3W	29	5.9	Andreanof Islands	68	7
9	31 Aug 72	14.03.16.3	52.3N	95.4E	33	5.5	Central Russia	44	61
10	07 Sep 72	02.54.58.3	2.0S	68.0E	33	5.8	Carlsberg Ridge	77	120
11	20 Oct 72	04.33.48.9	20.6N	29.7W	33	5.7	North Atlantic Ocean	49	234
12	20 Oct 72	08.17.48.6	18.8N	106.7W	38	5.7	Mexico	86	303
13	08 Nov 72	14.25.43.3	23.9N	121.6E	27	5.5	Taiwan	79	61
14	16 Nov 72	12.43.05.5	35.7N	69.9E	124	5.6	Hindu Kush	45	97
15	18 Dec 72	01.18.54.2	16.6S	28.1E	2	5.2	Zambia	79	163
16	27 Jun 73	03.15.20.4	43.1N	146.8E	45	5.0	Kurile Islands	70	33
17	27 Jun 73	03.42.38.0	42.6N	145.8E	38	5.2	Hokkaido, Japan	71	34
18	27 Jun 73	03.59.51.0	40.6N	89.5E	33	4.8	Southern Sinkiang	51	76

Table 2

The events used in this analysis. The hypocentral information is from the Preliminary Determination of Epicenters published by USGS (formerly NOAA, USCGS). The last two columns are distance and azimuth from NORSAR to the epicenter.

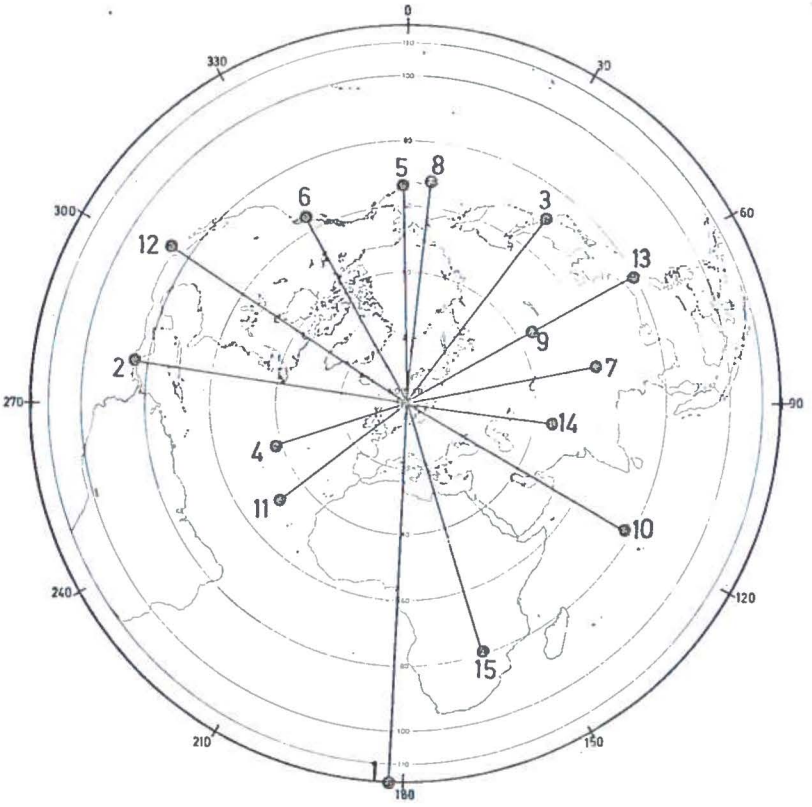

Fig. 6 The geographical locations of the events used in this analysis.

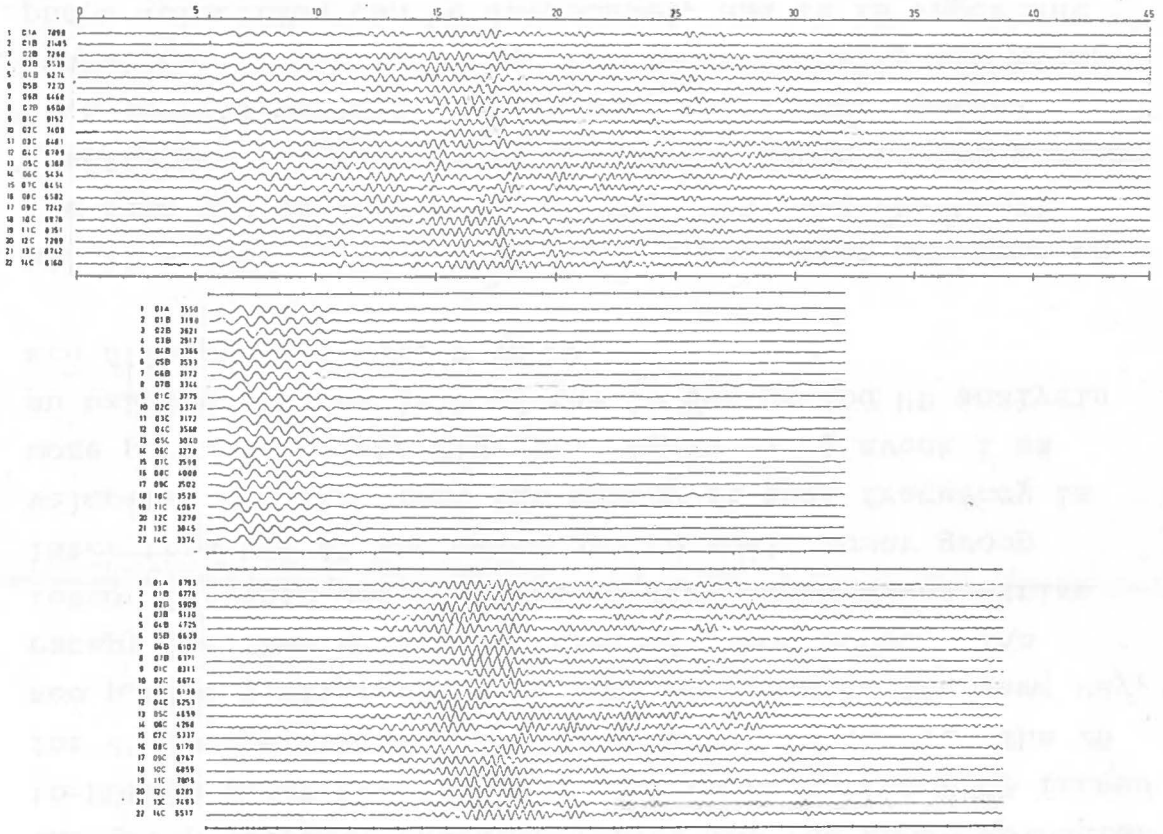

Fig. 7 Individual seismometer data for event no. 1. The first panel shows the unfiltered data, the next one is filtered around 40 sec and the bottom around 20 sec. The numbers following the subarray designation are scaling values in quantum units per unit deflection, and can be compared from one panel to the other.

For these reasons, one should expect the detectability to be better using 40 as compared to 20 sec period waves, provided the same signal energy is present at 40 sec as at 20 sec. These are assumptions which will be investigated in greater detail below.

Still using as an example the event shown in Fig. 7, the HR analysis was done in the following way. Eight successive non-overlapping 200 sec time intervals were analyzed using the 40 sec period prefiltered data. Each time interval was analyzed as 2 blocks each of 100 sec, and the first interval always started at the arrival time of the main 40 sec period group as computed from the group velocity characteristics for the known epicenter-to-NORSAR great circle path. For event 1, the 8 HR frames for 40 sec period are displayed in Fig. 8 (a-h). The 20 sec period prefiltered data were analyzed in the same way, except that two more time intervals were added. The reason for this was that the 20 sec period waves arrive later than the 40 sec waves due to their lower group velocity, and also that the energy at that frequency is more persistent (see Fig. 7). Again using event 1 as an example, frames 3-10 of the 20 sec period HR analysis are displayed in Fig. 9 (a-h).

All 15 events presented in Table 2 have been analyzed in the same way as shown through Fig. 7-9, and the basic results are given in Table 3. It was shown in the simulation results presented above that under some special conditions of multipathing, erroneous (usually too high) phase velocities can be introduced, and it is important to avoid a geophysical interpretation of such results. Also, the wavenumber quantization can introduce sizable errors in azimuth and phase velocity. The latter problem

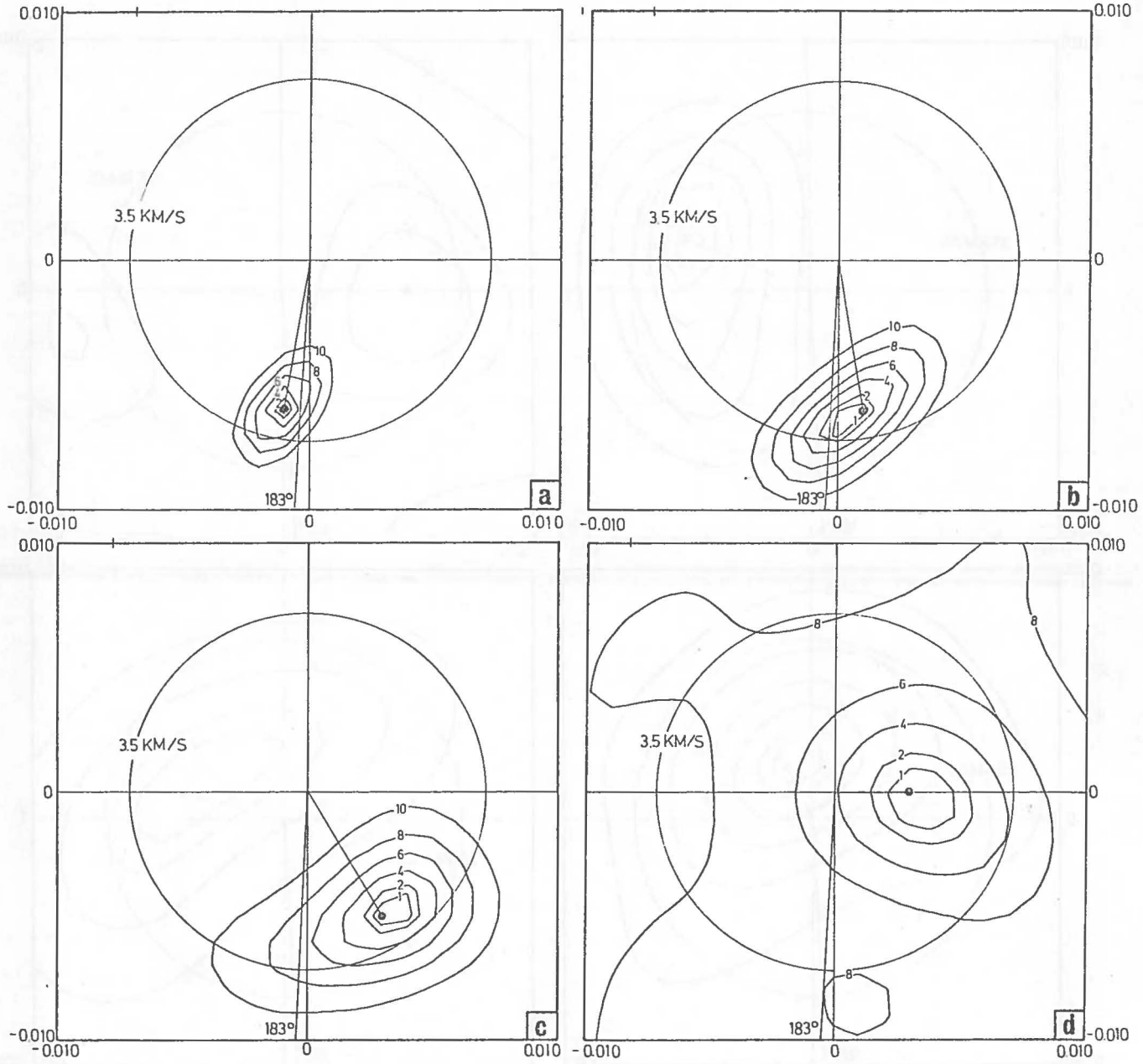

Fig. 8 Wavenumber spectra for 40 sec period data from event no. 1, shown in the second panel in Fig. 7. Frames a-h give the results for 8 consecutive non-overlapping blocks each of 200 sec, and the results are summarized in Table 3. The true azimuth to the event is indicated (183^{O}).

(cont.)

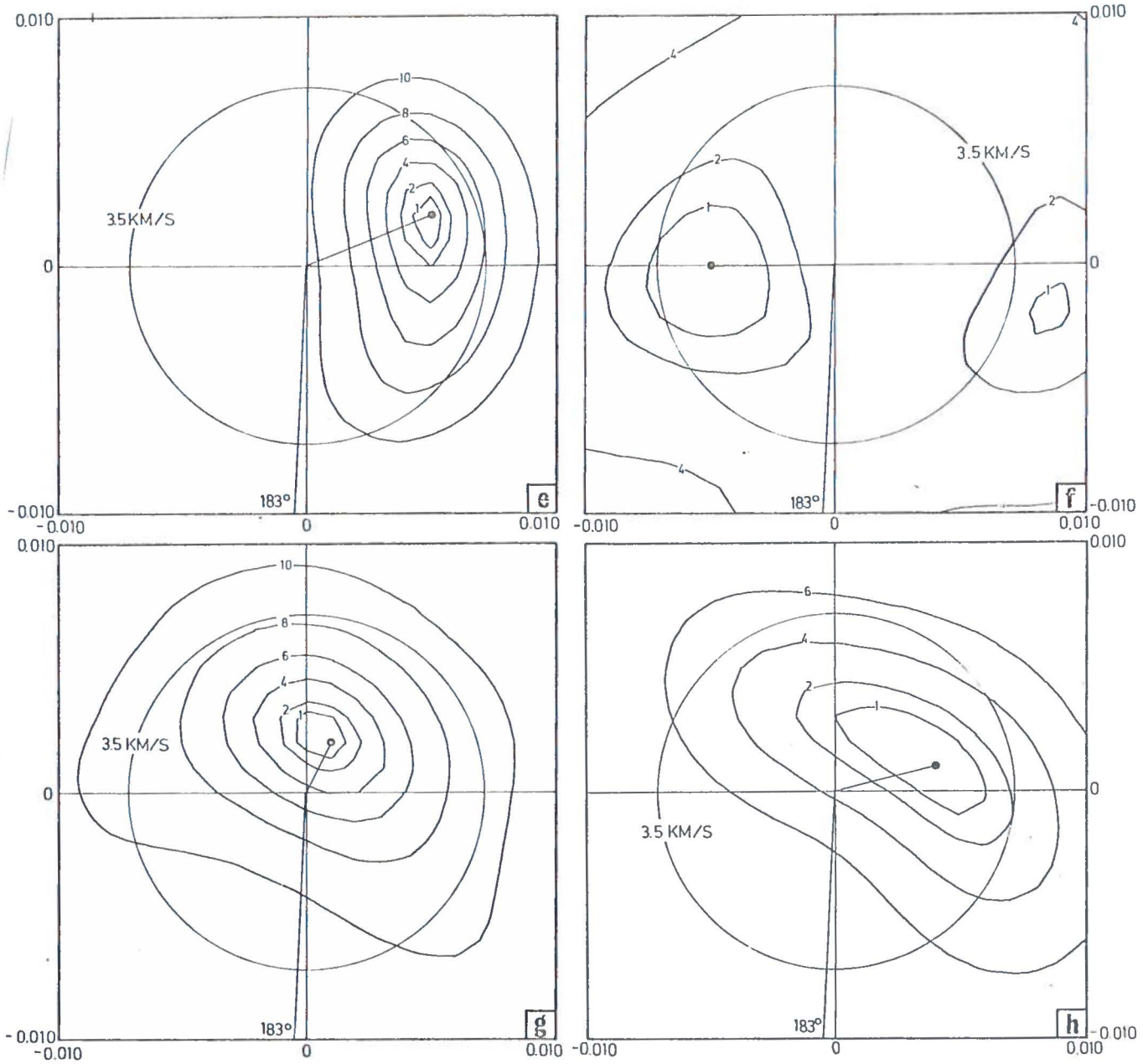

Fig. 8 (Cont.)

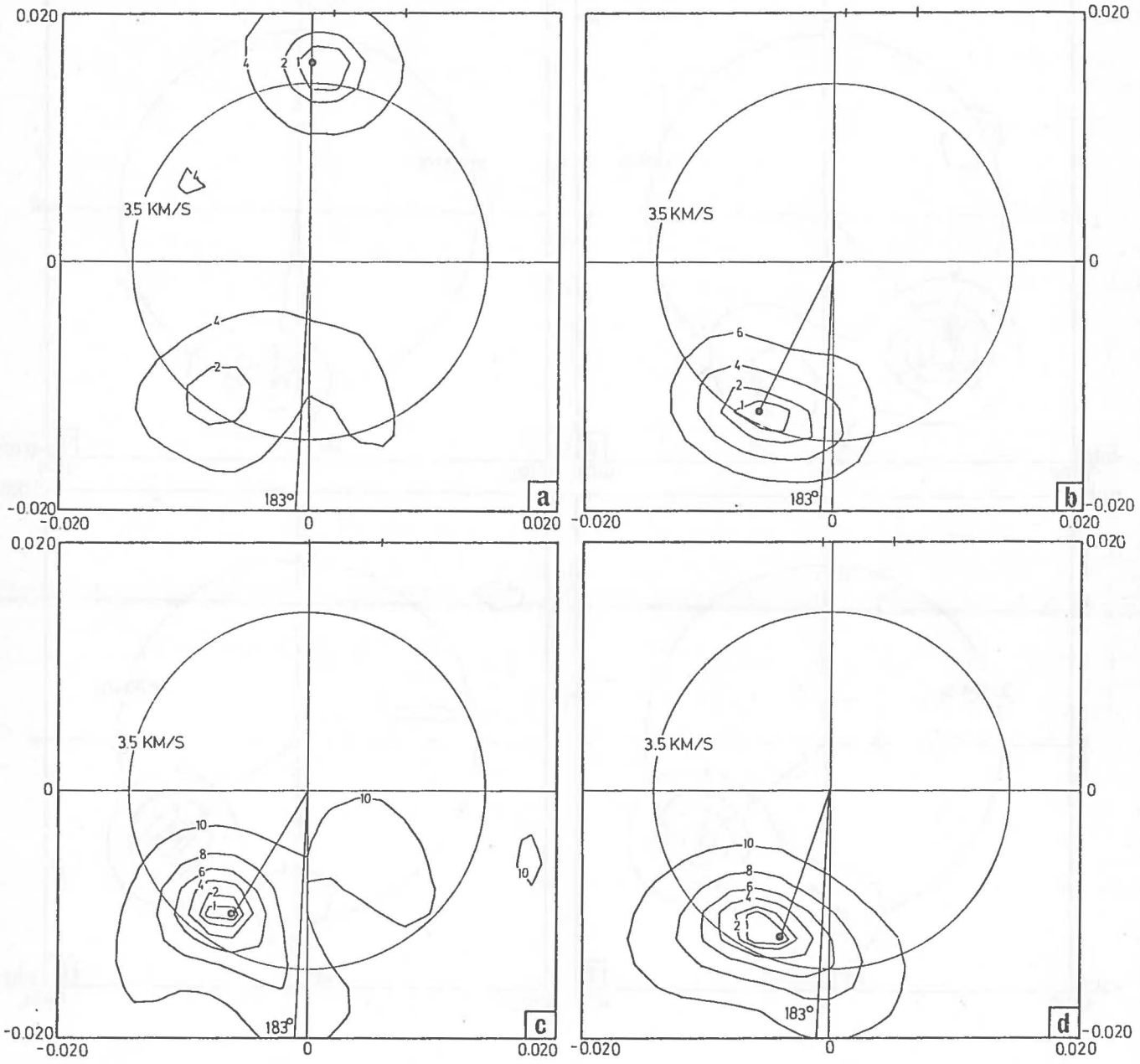

Fig. 9 Wavenumber spectra for 20 sec period data from event no. 1, shown in the second panel in Fig. 7. Frames a-h give the results for 8 consecutive non-overlapping blocks each of 200 sec, and the results are summarized in Table 3. The true azimuth to the event is indicated (183°).

(cont.)

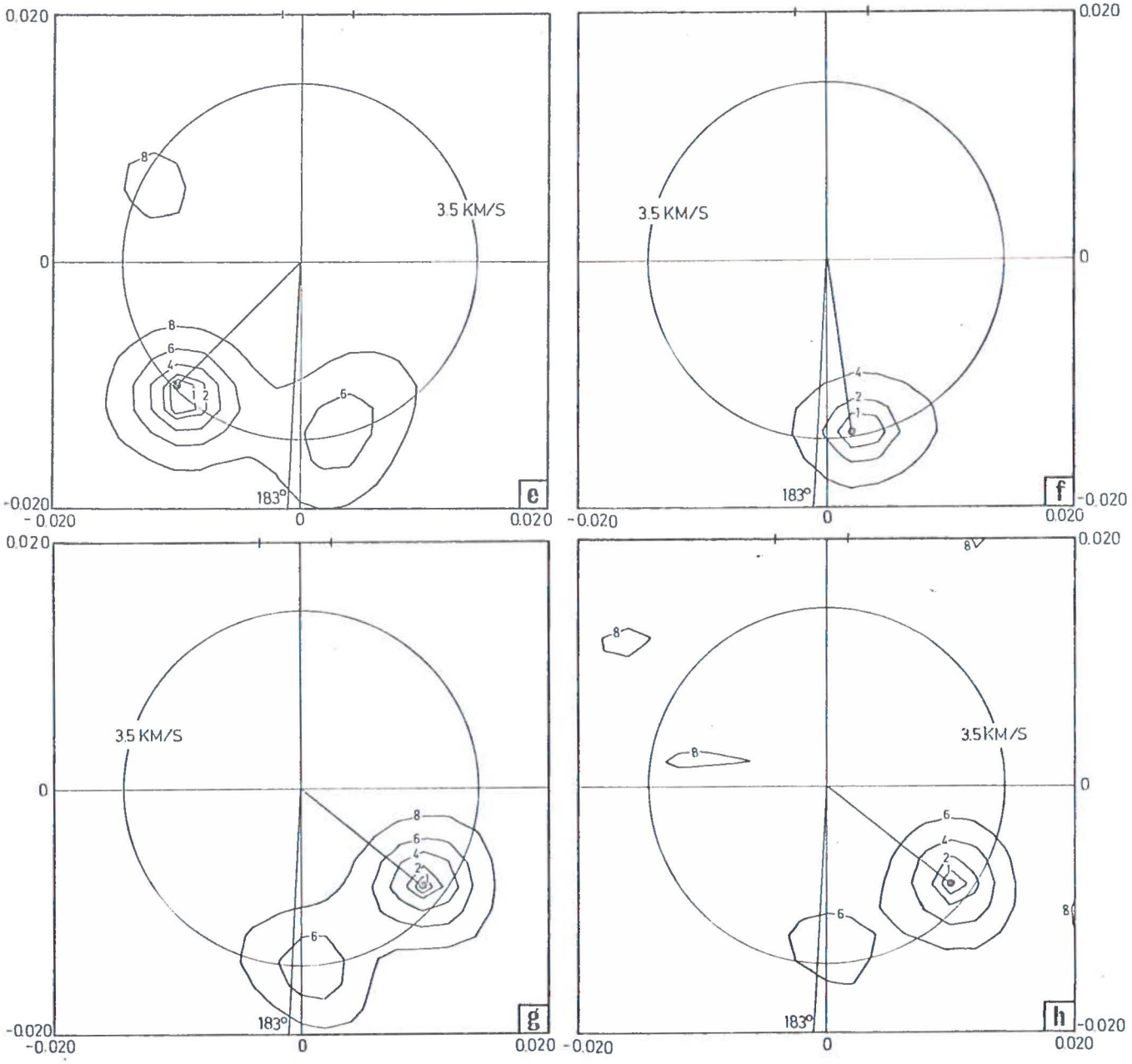

Fig. 9 (Cont.)

is treated in greater detail in the Appendix, where it is found, upon certain assumptions about expected phase velocities, that the accepted phase velocity range for 40 sec period Rayleigh waves at NORSAR is 3.5 - 4.2 km/sec and for 20 sec period waves 3.4 - 4.0 km/sec. This is the reason why, for example, azimuth and phase velocity have been accepted only for the first two 40 sec frames from event 1, while Fig. 8 shows that most of the other frames also have relatively well-defined concentrations of energy. At 20 sec period, Table 1 shows that 5 of the 7 frames after the arrival of the main group have been accepted and the results for the other events also support the assumption that there is more multipathing at 20 sec.

The distribution of power in the Rayleigh wave coda is given in Table 3, and also depicted in Figs. 10 and 11. Fig. 11 shows that the arrival of the main 20 sec group occurs between 1 and 4 frames (≈3-10 min) after the arrival of the 40 sec period waves, depending upon the amount of dispersion in the signal. It is also seen that there is significant amounts of 20 sec period energy arriving before the main group, and Table 3 shows that those early arrivals very often have valid Rayleigh wave phase velocities. Because of the prefiltering, this energy cannot possibly all be leaking in from lower frequencies, so that a more likely explanation is that this Rayleigh wave energy is originated through mode conversion from phases like multiply reflected P and S waves.

Another view of the power distribution is given in Fig. 12, showing the average results for the 15 events and the standard deviations for both the 40 and 20 sec period Rayleigh wave codas. One can see that after 6-7 minutes, the 40 sec period power has dropped 7-8 dB more than the

TABLE 3

Summarized results for the HR wavenumber analysis of the 15 first events in Table 1. Eight blocks of 40 sec data are analyzed and ten blocks of 20 sec data. The power level relative to the first block is given as well as the azimuthal deviation and phase velocity. One asterisk means that no significant peak in wavenumber space has been found, which also includes cases when the phase velocity is anomalous. Two asterisks indicate that the noise level has been reached (only events 4 and 9).

Event No.	Block No.	40 sec			20 sec		
		Azimuth deviation (deg)	Power (dB)	Phase velocity (km/s)	Azimuth deviation (deg)	Power (dB)	Phase velocity (km/s)
1	1	6	0	4.1	*	19	
	2	-12	5	4.1	24	18	3.7
	3	*	17		*	11	
	4	*	21		15	0	4.0
	5	*	22		42	6	3.5
	6	*	27		-11	9	3.5
	7	*	22		-54	11	3.9
	8	*	26		-54	13	3.9
	9				*	18	
	10				*	15	
2	1	0	0	4.1	*	22	
	2	-1	15	3.5	-1	11	3.5
	3	-9	10	4.2	9	0	4.0
	4	*	16		18	5	3.7
	5	*	15		18	9	3.7
	6	*	21		-9	9	3.6
	7	*	21		*	13	
	8	*	22		*	15	
	9				*	16	
	10				126	14	3.5
3	1	2	0	3.9	*	21	
	2	-3	3	3.5	2	15	3.9
	3	*	19		*	8	
	4	62	29	4.1	-10	2	3.7
	5	53	27	3.6	-21	0	3.4
	6	*	31		-3	11	3.5
	7	61	29	3.5	8	17	3.5
	8	61	26	3.5	*	18	
	9				*	19	
	10				*	17	
4	1	*	0		*	1	
	2	8	16	4.1	1	0	3.4
	3	-82	24	4.1	17	9	3.6
	4	*	21		-34	10	3.9
	5	*	22		-57	9	3.4
	6	*	24		-28	12	3.5
	7	*	24		*	14	
	8	**	26		*	16	
	9				*	14	
	10				*	14	
5	1	1	0	3.6	*	16	
	2	*	14		*	1	
	3	-8	19	4.1	1	0	3.6
	4	*	24		-17	4	4.0
	5	*	23		46	10	3.5
	6	*	28		35	9	3.5
	7	*	30		*	18	
	8	130	25	3.9	*	16	
	9				*	17	
	10				*	17	

TABLE 3

(cont.)

Event No.	Block No.	40 sec			20 sec		
		Azimuth deviation (deg)	Power (dB)	Phase velocity (km/s)	Azimuth deviation (deg)	Power (db)	Phase velocity (km/s)
6	1	2	0	3.7	*	14	
	2	*	6		*	0	
	3	*	20		29	2	3.6
	4	*	24		11	0	4.0
	5	56	21	3.7	*	2	
	6	-61	24	4.2	2	6	3.7
	7	*	29		*	4	
	8	*	27		63	10	3.5
	9				*	15	
	10				*	16	
7	1	9	0	3.6	*	7	
	2	17	0	3.5	-7	0	3.4
	3	9	4	4.2	*	5	
	4	27	6	4.0	27	5	4.0
	5	27	16	4.0	*	13	
	6	*	14		36	11	3.7
	7	*	15		*	15	
	8	*	23		*	16	
	9				*	16	
	10				*	19	
8	1	1	0	3.5	*	16	
	2	27	10	3.5	*	3	
	3	*	15		-15	0	3.5
	4	*	20		11	3	4.0
	5	-79	23	4.0	38	2	3.5
	6	128	21	3.5	-34	7	3.7
	7	*	23		*	14	
	8	101	21	4.0	*	19	
	9				*	15	
	10				*	16	
9	1	2	0	3.7	11	12	4.0
	2	*	13		-5	0	3.5
	3	*	19		-69	5	3.5
	4	29	17	3.6	-34	9	3.7
	5	**	20		-45	13	3.4
	6	**	24		*	13	
	7	**	24		*	16	
	8	**	22		63	15	3.5
	9				-69	19	3.5
	10				*	23	
10	1	3	0	3.7	*	20	
	2	-12	6	4.0	9	15	3.9
	3	22	13	3.5	15	4	3.5
	4	-30	17	3.6	-3	2	3.7
	5	*	25		-12	0	4.0
	6	*	28		-12	6	4.0
	7	*	23		-14	9	3.4
	8	*	29		-38	9	3.5
	9				*	8	
	10				*	14	

TABLE 3

(Cont.)

Event No.	Block No.	40 sec			20 sec		
		Azimuth deviation (deg)	Power (dB)	Phase velocity (km/s)	Azimuth deviation (deg)	Power (dB)	Phase velocity (km/s)
11	1	-3	0	3.9	*	15	
	2	-36	13	4.0	-3	0	3.9
	3	*	19		-9	14	3.5
	4	*	19		-20	16	3.5
	5	*	19		*	21	
	6	*	26		*	28	
	7	*	21		-15	29	3.9
	8	*	23		*	30	
	9				*	25	
	10				*	31	
12	1	12	0	3.5	*	14	
	2	*	8		-6	3	3.7
	3	39	15	4.0	-17	0	3.4
	4	48	19	4.1	*	0	
	5	*	25		30	1	3.7
	6	96	24	3.9	30	2	3.7
	7	*	28		65	9	3.5
	8	*	29		57	12	3.6
	9				*	12	
	10				*	16	
13	1	2	0	3.7	*	28	
	2	37	17	3.5	*	17	
	3	*	19		*	6	
	4	47	15	4.0	*	0	
	5	20	17	4.1	11	14	4.0
	6	*	20		-22	17	3.9
	7	*	21		*	18	
	8	*	20		*	23	
	9				*	26	
	10				*	26	
14	1	2	0	4.1	1	3	3.5
	2	1	8	3.5	11	6	4.0
	3	-7	24	4.2	1	0	3.5
	4	*	29		9	11	3.4
	5	*	30		1	14	3.5
	6	*	30		*	19	
	7	*	32		*	19	
	8	*	31		*	22	
	9				*	20	
	10				*	12	
15	1	-10	0	3.7	-1	12	4.0
	2	-22	4	3.9	17	7	3.6
	3	51	8	3.5	-1	1	4.0
	4	*	13		25	0	3.5
	5	*	17		25	4	3.5
	6	*	17		*	4	
	7	*	18		51	6	3.5
	8	*	16		73	12	3.5
	9				*	12	
	10				*	14	

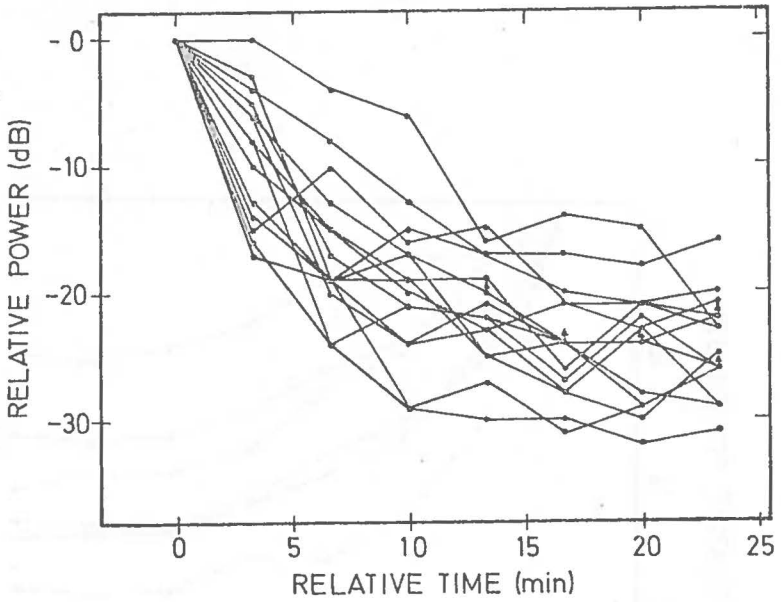

Fig. 10 40 sec period coda power relative to the block with maximum power (always block no. 1). The actual numbers are given in Table 3.

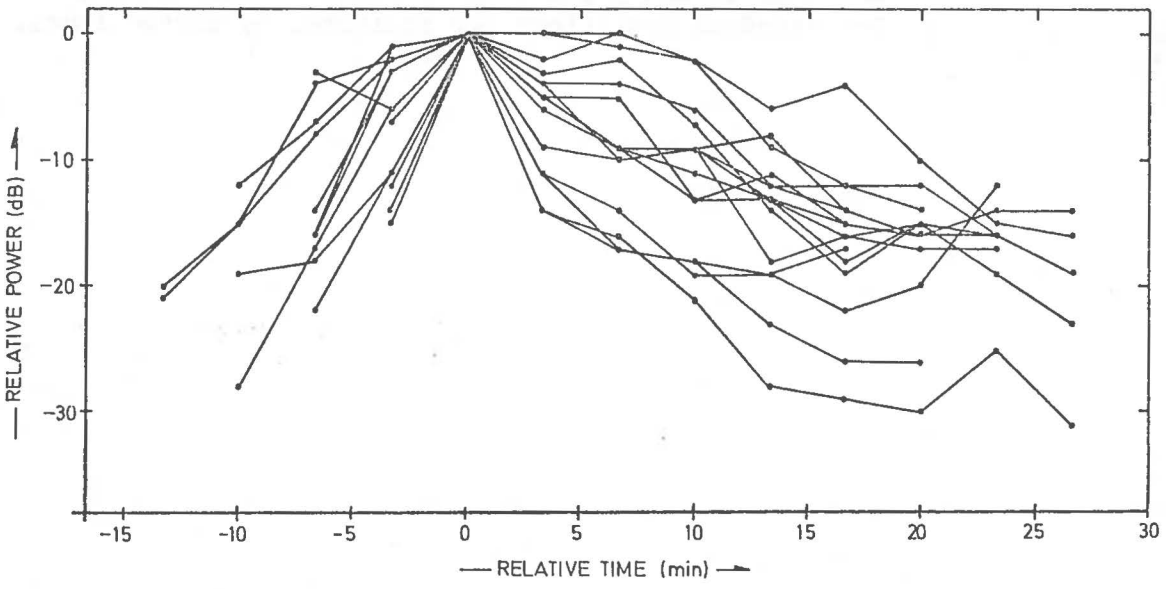

Fig. 11 20 sec period coda power relative to the block with maximum power. The actual numbers are given in Table 3.

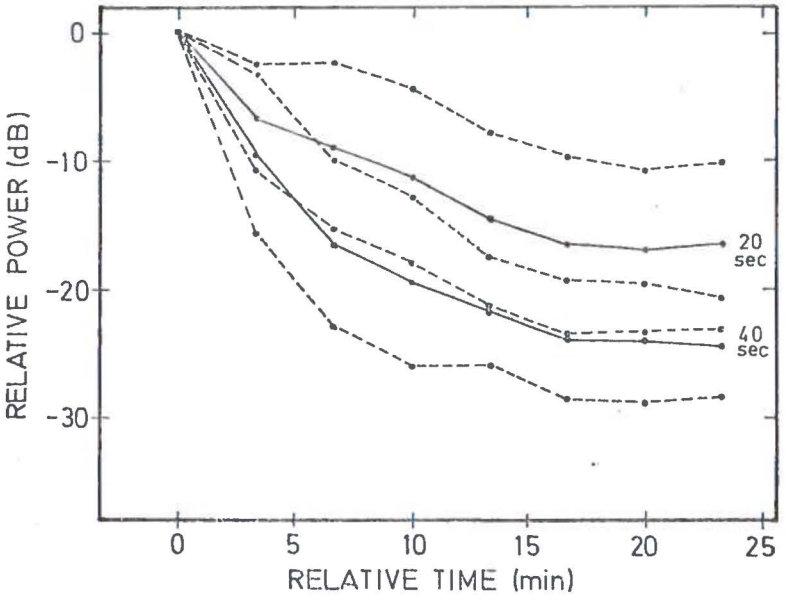

Fig. 12 The average of the coda power distributions displayed in Figs. 10 and 11, for the periods 40 and 20 sec. The standard deviations are indicated by dotted lines.

20 sec power, whereafter the difference is about constant. The standard deviation is in the range 4-6 dB for both frequencies. The results summarized in Fig. 12 should normally mean that by analyzing at 40 rather than at 20 sec period, the detection of the Rayleigh waves would not as often be obscured by an interfering event provided there is equal signal energy at these two periods. Another argument that also favors the 40 sec period is the observation that there is more multipathing at 20 sec. On the other side, however, is the fact pointed out above that the HR method works better at 20 sec, due to the improved array response. In addition, the signal-to-interference ratio may actually be better at 20 sec, if there is enough signal energy to compensate for the increased amount of interfering event energy at this period, relative to 40 sec. A general conclusion as to which frequency to use can therefore not be reached, and the detection at these two periods should be considered simultaneously.

RAYLEIGH WAVE MULTIPATH PROPAGATION

Besides the power distribution within the Rayleigh wave coda, Table 3 also gives the azimuthal deviations from the great circle path for all frames having an acceptable phase velocity. The column of azimuthal deviations clearly shows that there are considerable amounts of multipathing, and that deviations as large as 40 - 60 degrees are quite typical. A geophysical interpretation of some of those observations will now be offered.

In one of his works on surface wave multipathing at LASA, Capon (1970), see also Capon (1971) and Capon and Evernden (1971), has discussed the case of a dispersive wave train propagating across a boundary. After a number of simplifying assumptions, he showed that the dispersive wave train is refracted across a boundary according to Snell's Law for the respective phase velocities, and that

the total travel time is determined by the group velocities in the respective media. He also pointed out that the ray path must satisfy Fermat's principle, i.e., it must be a stationary time path. In the special case of the paths of initial arrivals, they will be minimum time paths.

All the ray path solutions presented below were obtained starting with the group velocities given by Oliver (1962). These are, for 40 sec period, 3.60 and 4.10 km/sec for continental and oceanic paths, respectively, and for 20 sec period, 2.95 and 3.70 km/sec. If other group velocities were used, it is mentioned specifically. In cases where there was an arrival along the great circle path, this gave a direct measurement of the group velocity, offering a possible adjustment to the reference values cited above. For the later arrivals, the restrictions were that the travel path differences relative to the other arrivals must be consistent with the respective travel time differences. This does not offer a unique solution, so two other restrictions were also imposed on the solutions; first, only one refraction or reflection was considered due to the energy involved, and second, a refraction or reflection was preferred when it occurred near a major geophysical boundary, usually a continental margin. For simplicity, these were usually considered to coincide with the outlines of the continents. The uncertainties involved in these travel path solutions are partly discussed in the Appendix, where it was demonstrated that there is an azimuth uncertainty of $\pm 5^{o}$ due to the wavenumber quantization. In addition to that there is the uncertainty introduced when there is power from several azimuths within the same 200 sec time interval, as discussed above in the chapter on simulated data.

There is also the simple geometrical fact that an azimuthal deviation of 10 degrees gives at most an additional 3% path

length, while 20 degrees gives 13%. This should be compared to the uncertainty introduced by the 200 sec between each wavenumber frame, which is 10-12% of the travel time at an epicentral distance of 60 degrees. These uncertainties should give the proper warning against giving too much significance to the finer details of the proposed ray path solutions.

Figs. 13-19 give the proposed ray path solutions for events 1, 2, 6, 8, 9, 12 and 15 in Tables 2 and 3. These seven events constitute a representative subset of the fifteen events analyzed, and most of the major seismic regions of the world are still covered. For event 1, the velocities of Oliver (1962) fitted quite well the solutions for both the period of 40 and 20 sec. At 40 sec period, the arrival at $+6^{\circ}$ (see Table 3) is the most uncertain; it could also have been refracted in the North Africa/Mediterranean area. The other arrival (-12°) leaves no other reasonable solution than a refraction near the southern tip of Africa. At a period of 20 sec, there is a refraction in the same area, while the arrival at -54° is observed over two wavenumber frames and thus can be reflected over a fairly large area. For event 2 (Fig. 14) the Oliver velocities have been used at 40 sec period, while the solutions for 20 sec period were obtained using an average group velocity of 3.4 km/sec, which is reasonable enough taking into consideration that portions of the paths are continental. Also, it appears that the group velocities over much of the Arctic ocean are more or less continental. This phenomenon is better observed for event 6 (Fig. 15), where the solutions for 40 sec period were obtained using a group velocity of 3.7 km/sec, and for 20 sec period 3.0 km/sec, both being very close to Oliver's values for continents.

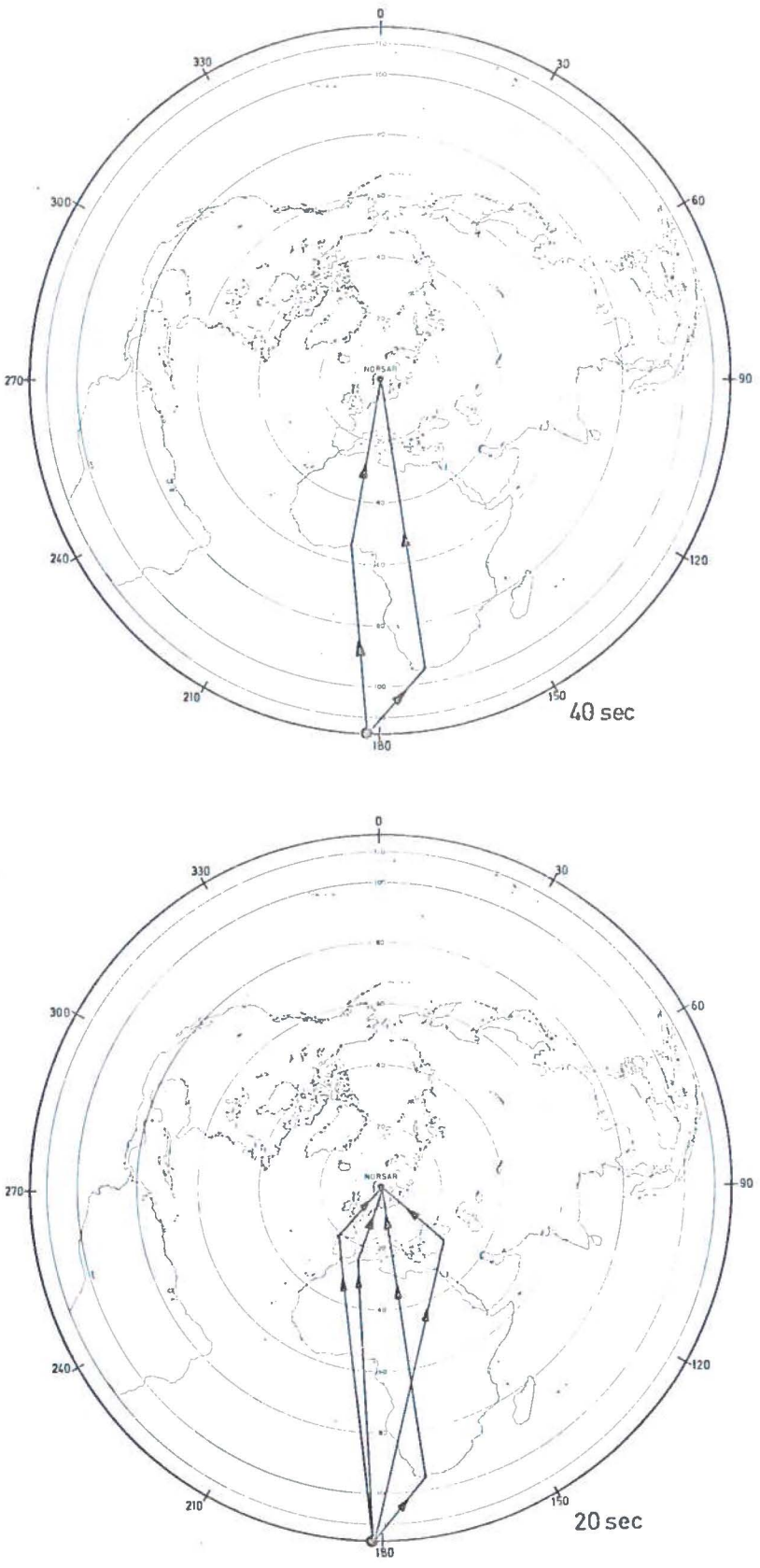

Fig. 13 Ray path solution for event no. 1, 40 and 20 sec period

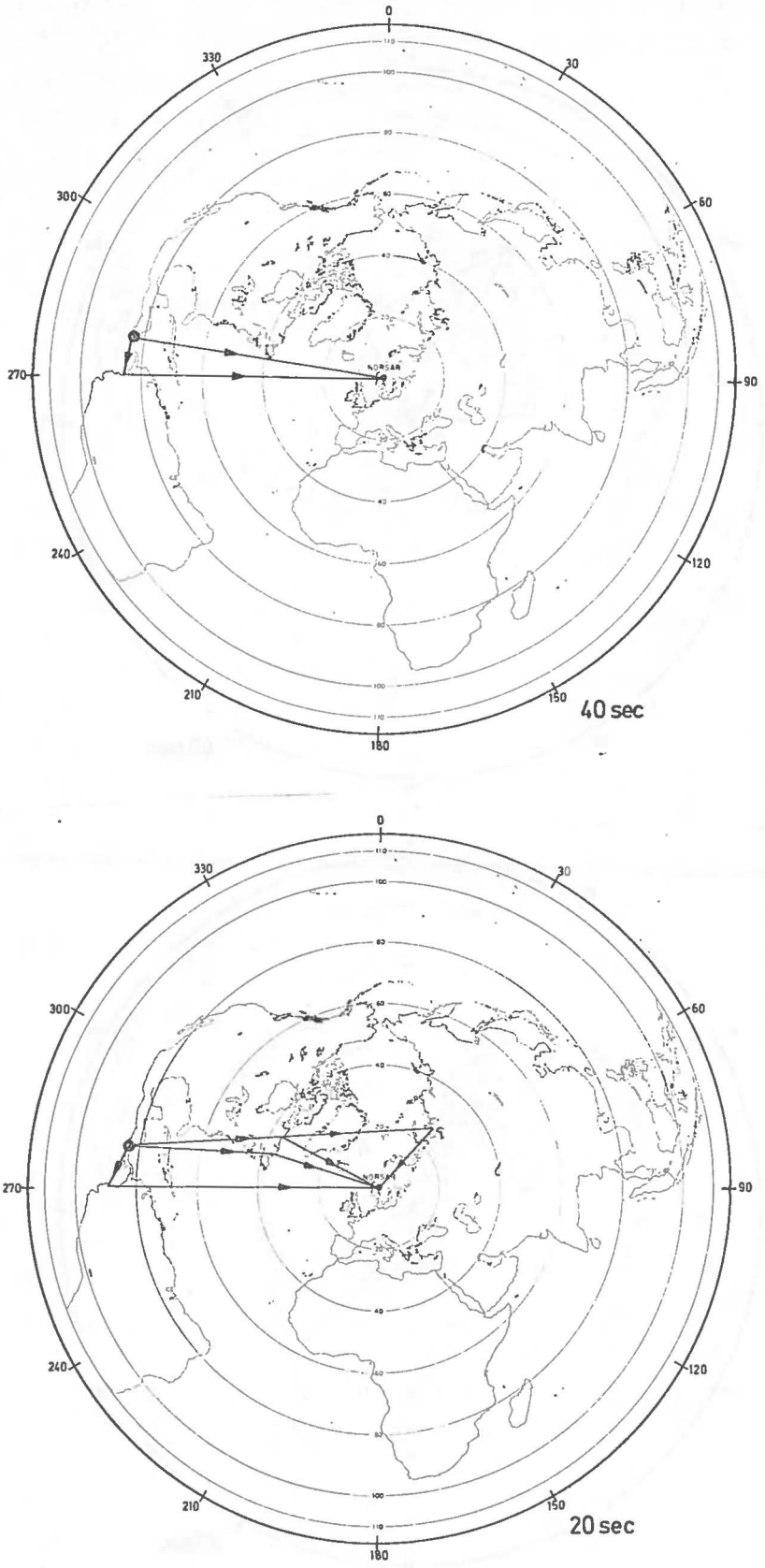

Fig. 14 Ray path solution for event no. 2, 40 and 20 sec period.

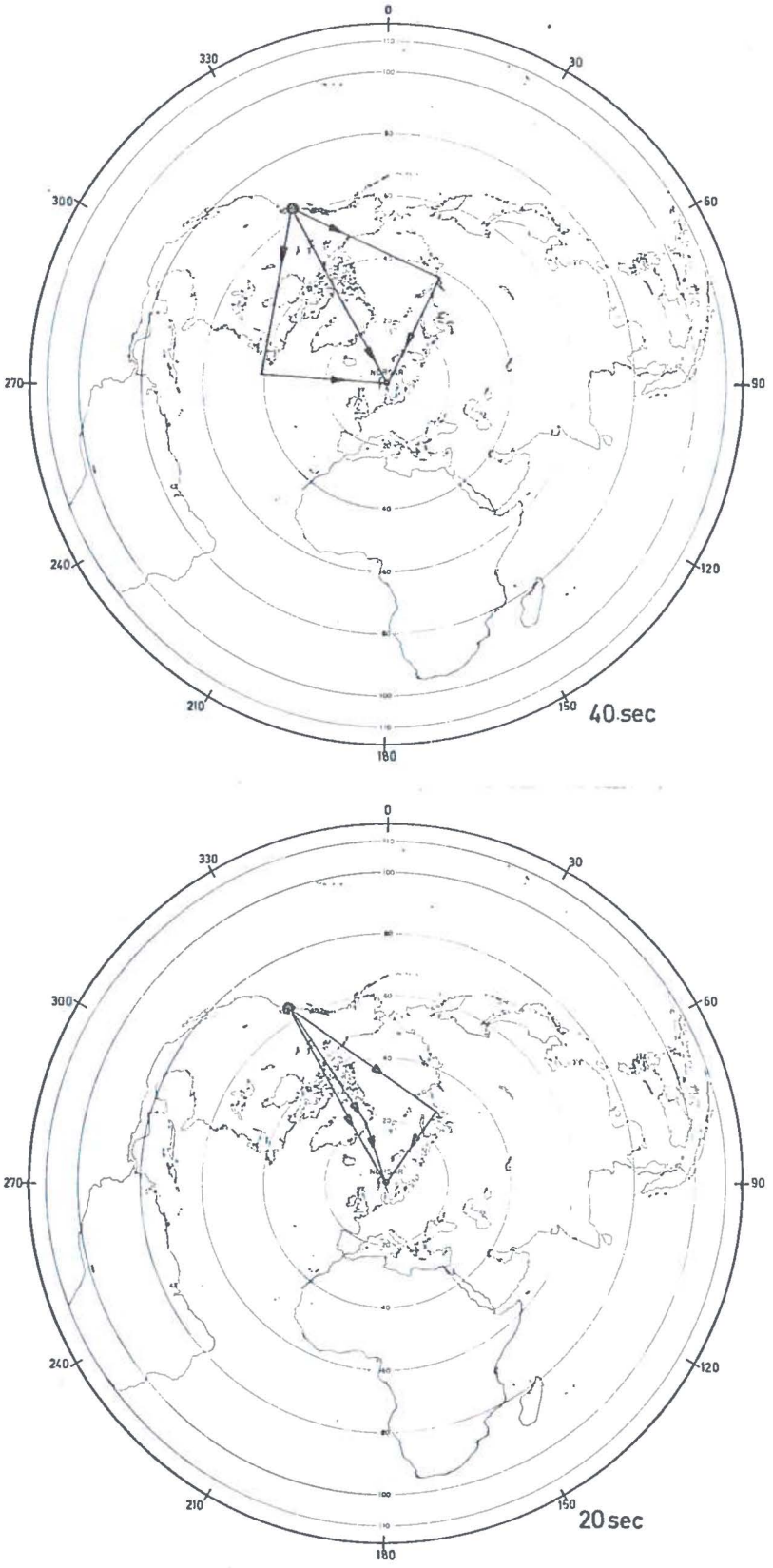

Fig. 15 Ray path solution for event no. 6, 40 and 20 sec period.

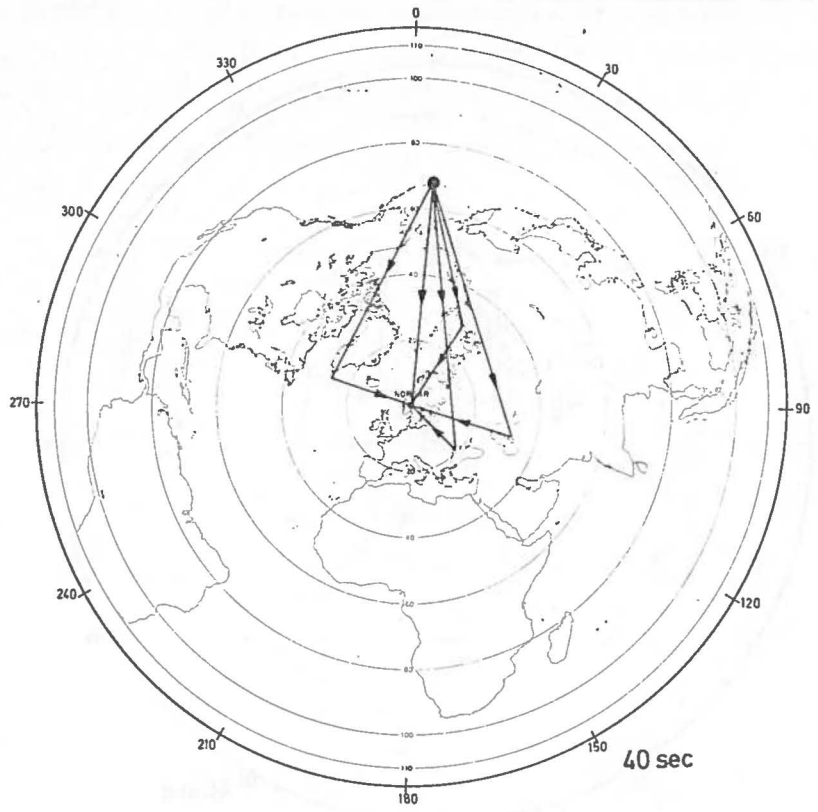

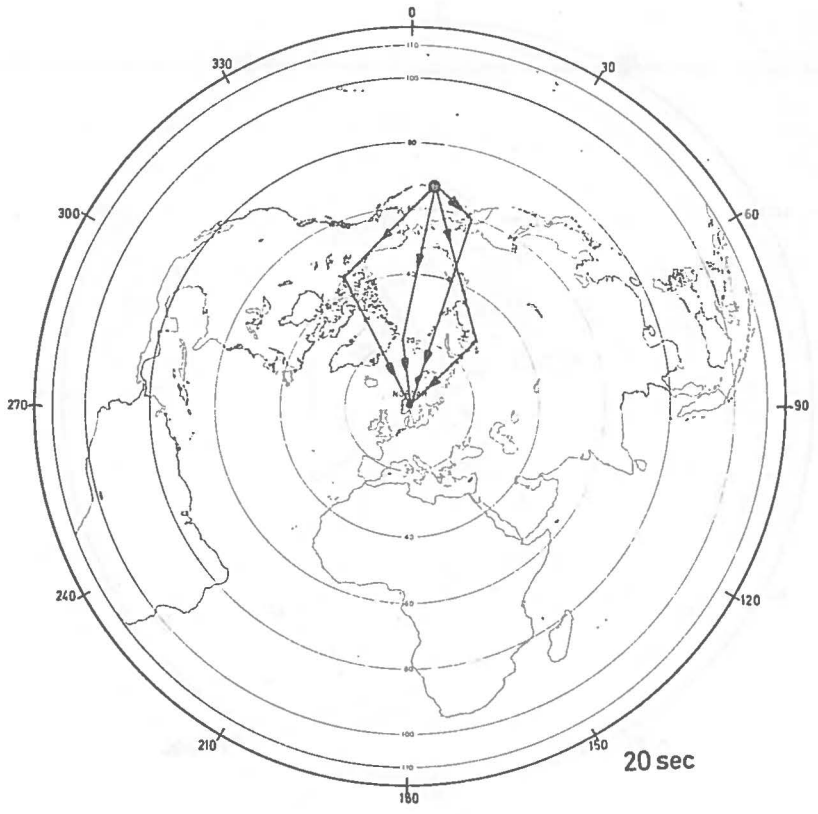

Fig. 16 Ray path solution for event no. 8, 40 and 20 sec period.

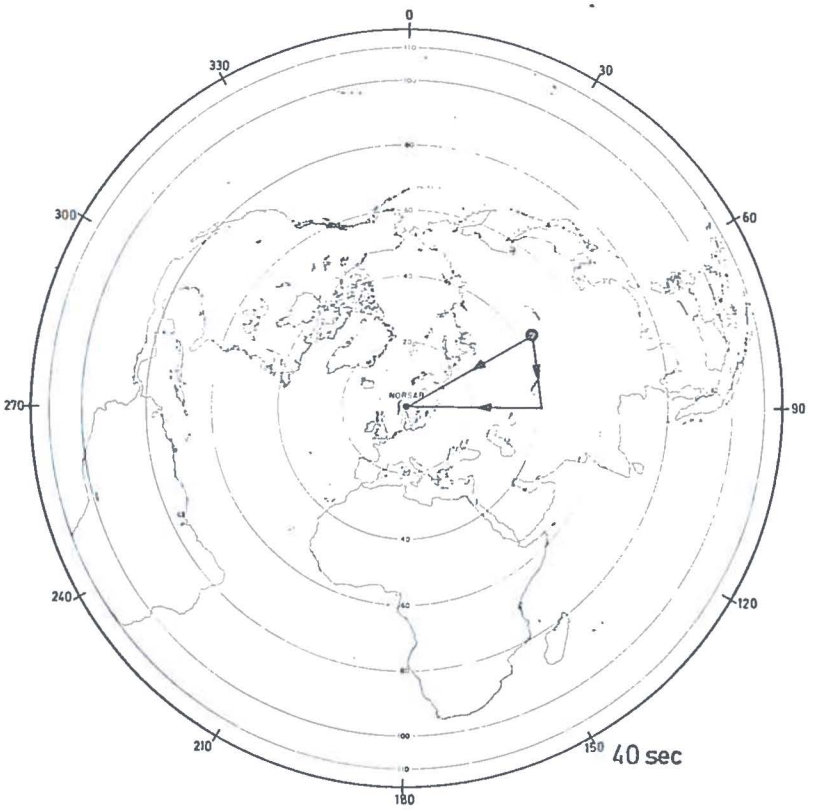

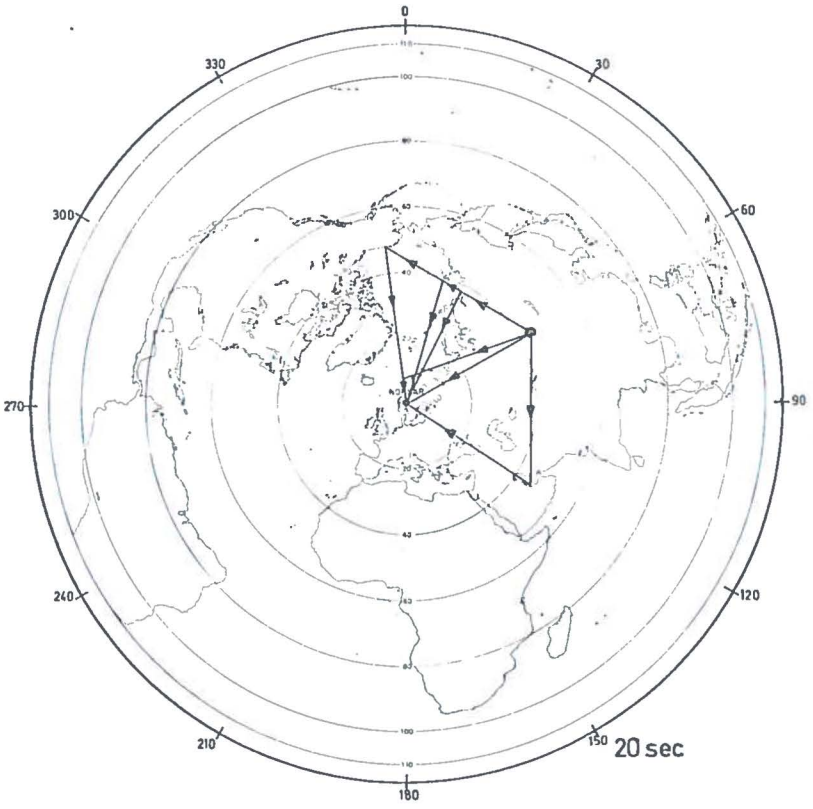

Fig. 17 Ray path solution for event no. 9, 40 and 20 sec period.

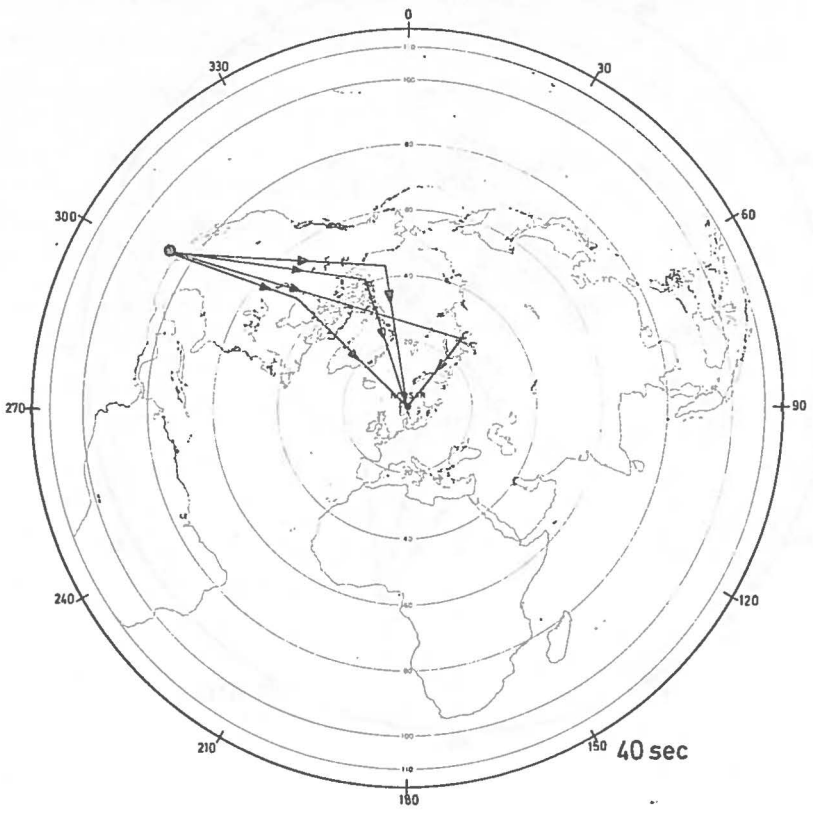

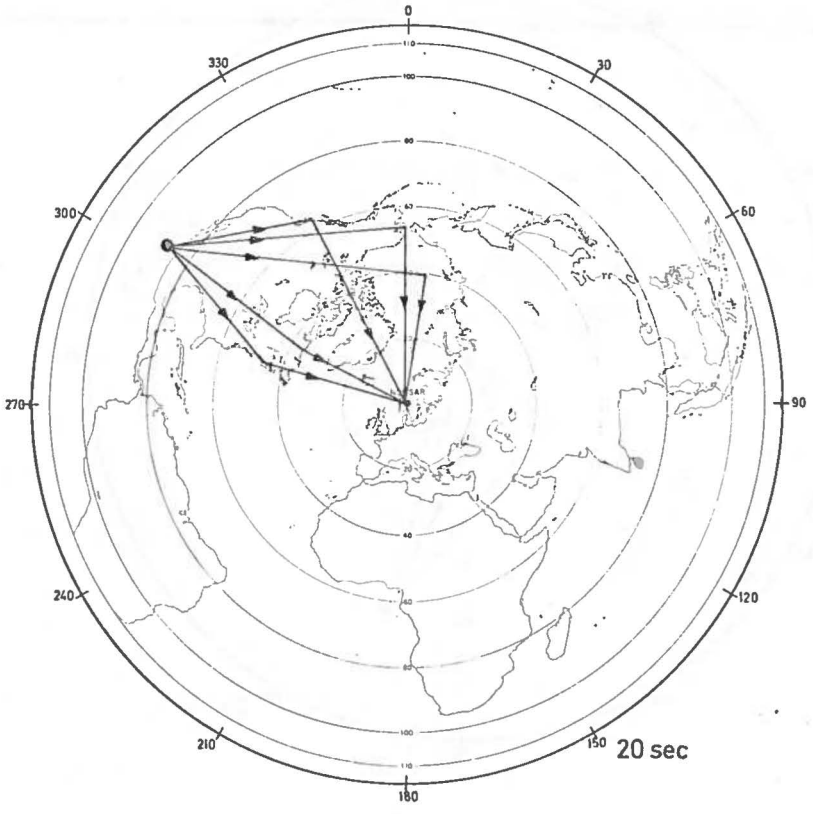

Fig. 18 Ray path solution for event no. 12, 40 and 20 sec period.

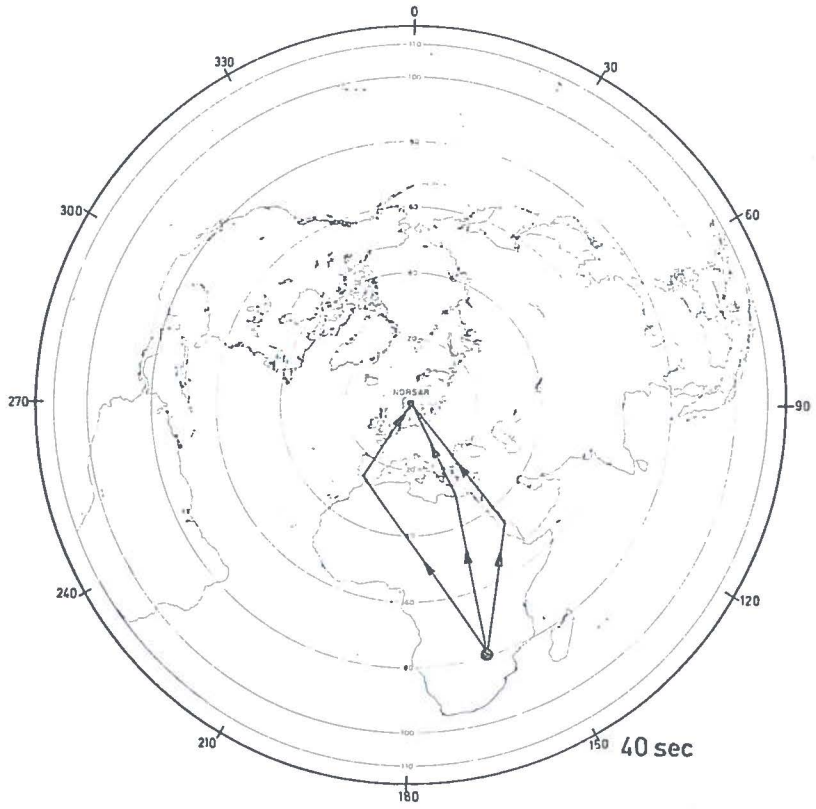

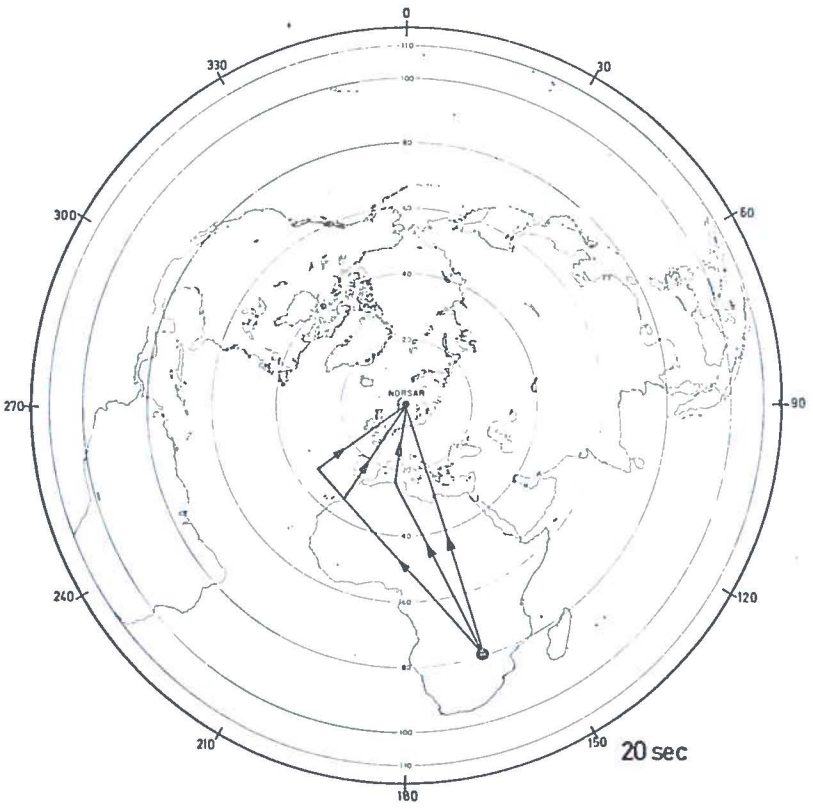

Fig. 19 Ray path solution for event no. 15, 40 and 20 sec period.

The 20 sec period power for this event is quite interesting, since it stays almost at the same level for six consecutive time intervals, or about 20 minutes. Also, some of that energy is so early that it cannot have propagated as Rayleigh waves all the way, which leaves, as mentioned above, mode conversion as a reasonable explanation. For event 8 (Fig. 16) the same near-continental velocities as for event 6 were the ones which gave the most reasonable solutions, also being consistent with the great circle arrivals. The scattering is quite severe, especially for 40 sec period, where the energy arrives over a sector covering 210°. At 20 sec period, the energy for this event is also very persistent, for 20 minutes it keeps arriving from all over the Arctic ocean area without any clearly defined great circle path arrival. Event 9 (Fig. 17) one should think could not give much multipathing, which is certainly true at 40 sec period. At a period of 20 sec, however, there are, besides the great circle arrival (at -5°), a number of well-defined later arrivals, and the Arctic ocean again seems to be contributing significantly to the scattering. Also this time, these areas had to be considered continental with respect to group velocities, which also was the case for event 12 (Fig. 18), where a large number of arrivals from a wide azimuthal range have been accepted. The solutions obtained all seem to be associated with refractions and reflections at some geophysical boundary, in addition to which they are internally consistent. In our last example, event 15 (Fig. 19), we are almost back to where we started in Fig. 13, and there are also certain similarities between the multipathing for the two events. The group velocities used this time were also those of Oliver (1962).

DETECTION OF ATMOSTPHERIC EXPLOSIONS

A number of independent sources reported that an atmospheric nuclear explosion took place at the Lop Nor test site in China on 27 June 1973. This explosion, identified in this paper as event 18 (Table 2, Fig. 20), can be used as a good example in trying out the detection method outlined above. This is because the event occurred in the middle of an earthquake swarm from the Kurile Islands/ Hokkaido region, and the expected arrival time for the explosion Rayleigh waves coincided exactly with the Rayleigh waves from one of the earthquakes in the swarm (event 17). Also, an event with hypocentral parameters quite close to the interfering event occurred half an hour before, which made it an ideal reference event (event 16). All these events, the reference event, the interfering event, and the explosion are listed in Table 2 (event 16-18) and depicted in Fig. 20.

In accordance with the procedure outlined above, both the 40 and 20 sec period groups have been analyzed using the HR method applied to prefiltered data. The results for 40 sec period are shown in Fig. 21, where the HR spectra from four consecutive 200 sec time intervals are depicted. The main 40 sec period group arrives in the second frame (b), and is also presented in the third frame (c) before it fades away. No multipathing is seen in those two frames, and the azimuth coincides almost exactly with the direction towards the explosion. We conclude therefore that the energy at 40 sec period is completely dominated by the explosion.

At 20 sec, however, the picutre is quite different. Fig. 22 shows the HR results for the reference event, and Fig. 23 gives the results for the desired plus interfering events, and the two should be studied simultaneously. The start

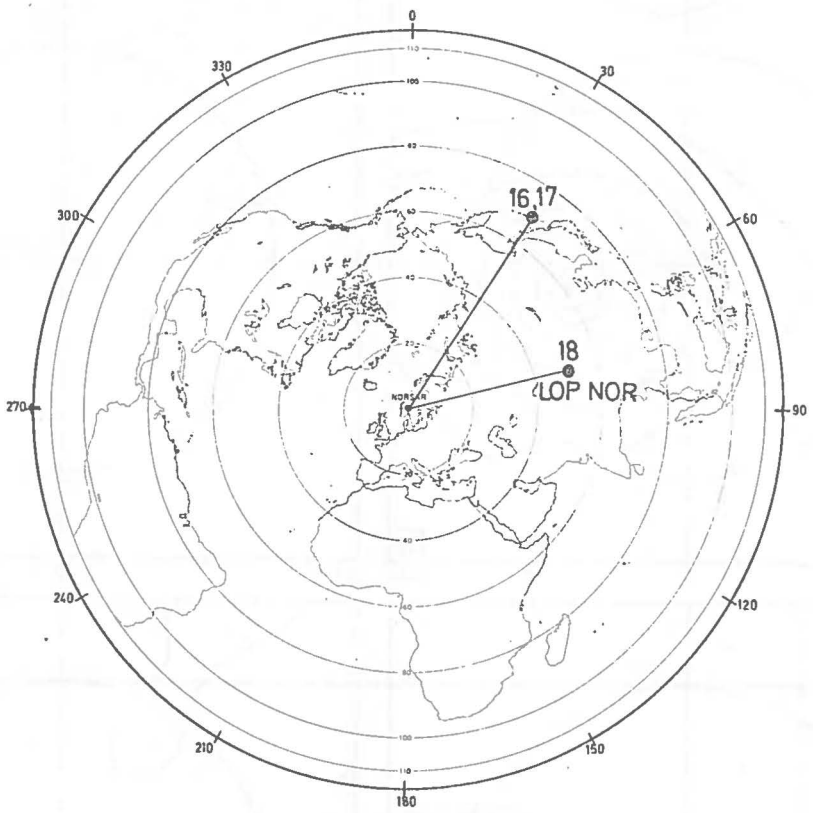

Fig. 20 The geographical locations of events 16-18 in Table 2.

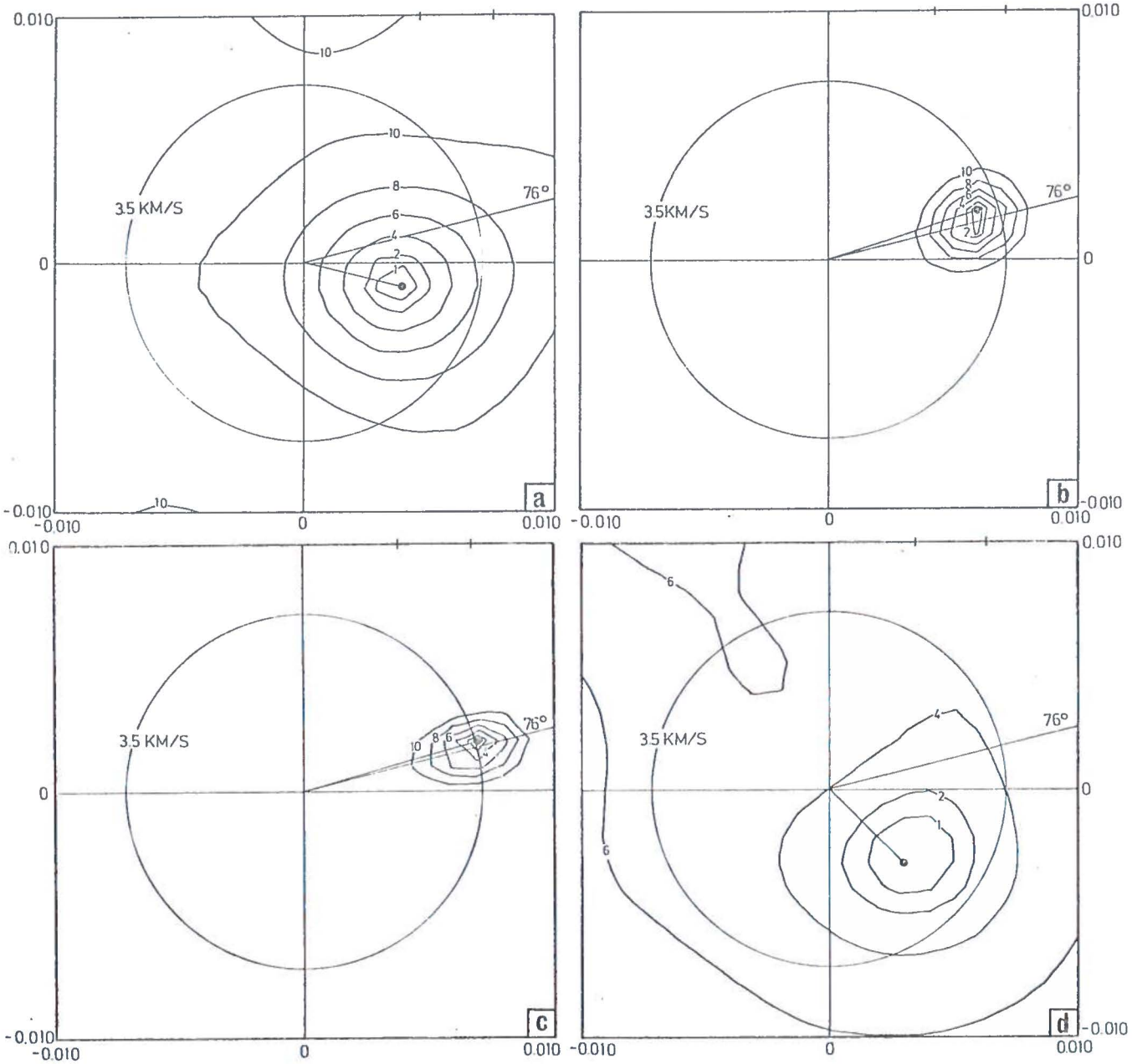

Fig. 21 Wavenumber spectra at 40 sec period for the Lop Nor explosion (no. 18). The energy from the interfering event (no. 17) cannot be seen.

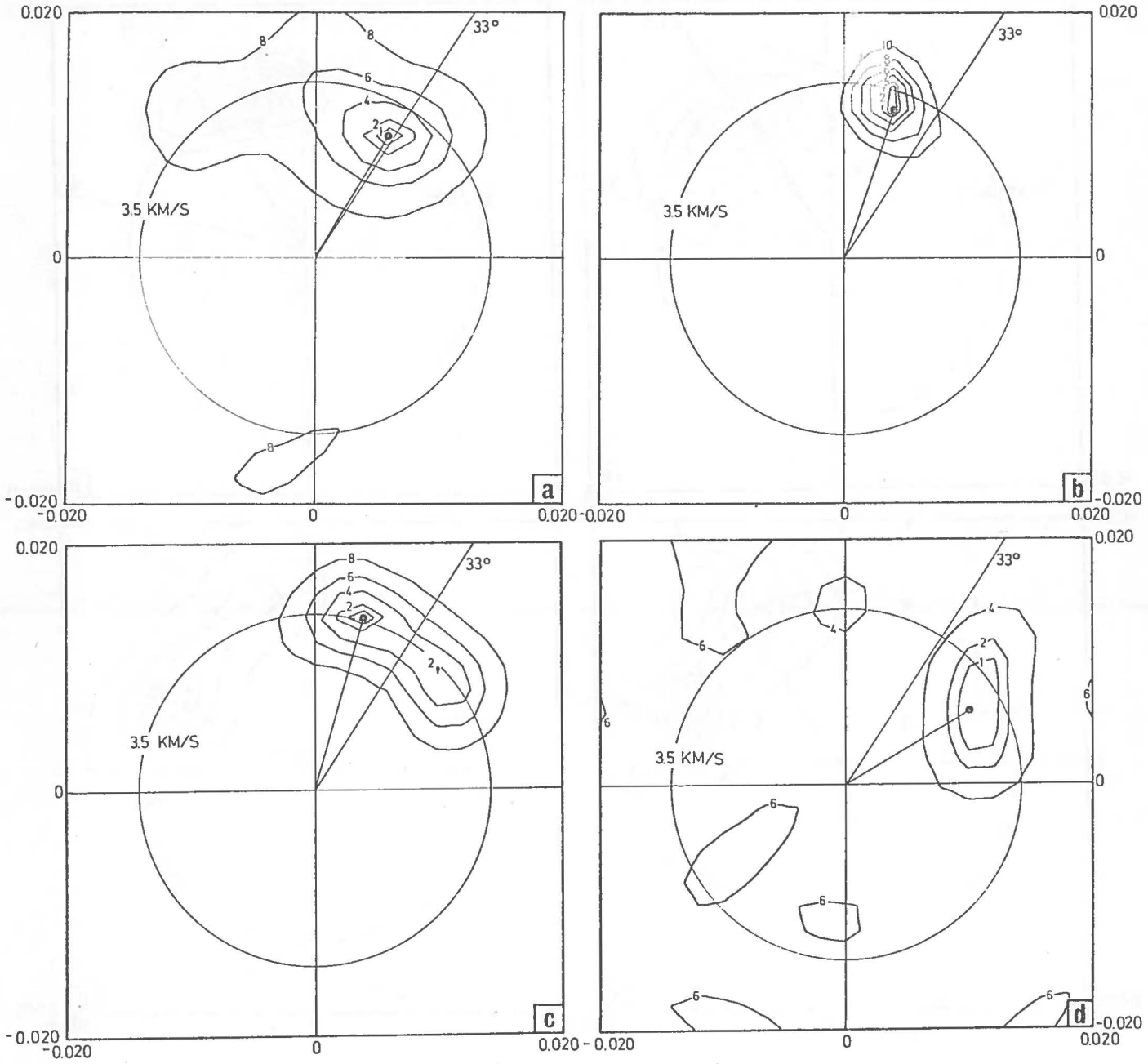

Fig. 22 Wavenumber spectra at 20 sec period for the reference event (no. 16). The true azimuth to this is indicated (33°).

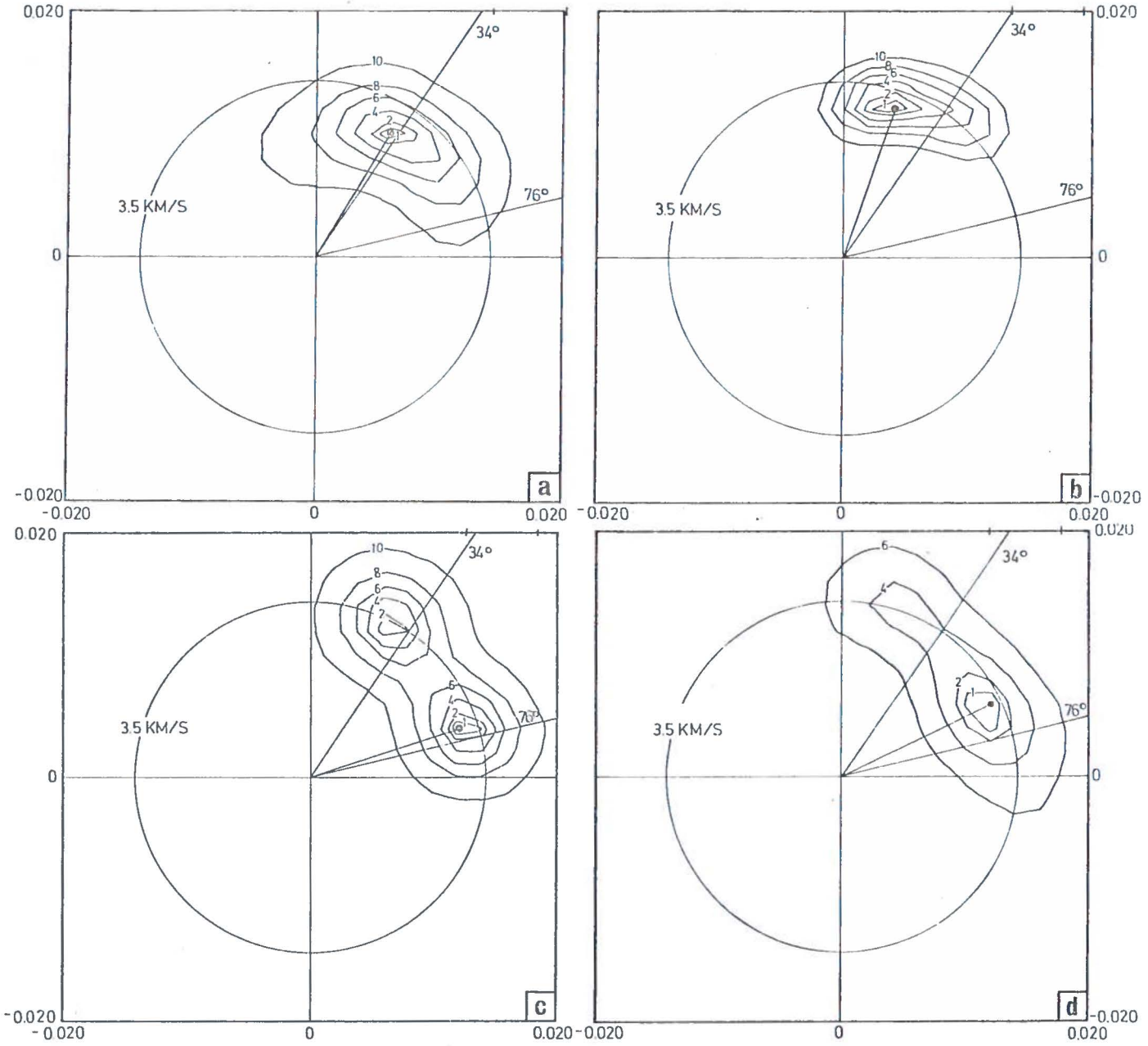

Fig. 23 Wavenumber spectra at 20 sec period for the Lop Nor explosion (no. 18) and the interfering event (no. 17). The true azimuths for these events are indicated (76^{o} and 34^{o}).

times of the two figures are the same relative to the reference event and the interfering event, respectively. In frame one (a), the azimuth points directly to the reference/interfering event, although the phase velocity is somewhat too high (4.3 km/sec). In the next frame (b), the azimuth decreases for both events, possibly favoring a reflection somewhere in northern Siberia (see Fig. 20), and the explosion is not seen. In Fig. 22c there is a slight multipathing at about 45 degrees, while in Fig. 23c the main energy now comes from an azimuth pointing towards Lop Nor, which firmly establishes the detection of the explosion. In the last frame (d), Fig. 23 still has some energy which probably is from the explosion, while the reference event only has some weak multipathing with erroneously high phase velocity.

DISCUSSION

All the data analysis in the present study has been done using the HR method of estimating the power of Rayleigh waves in frequency-wavenumber space. Using this technique, we are faced with a number of limitations which it is essential to keep in mind during the interpretation of the results. These limitations, which have been discussed in various connections above, are essentially the following:

Short time intervals

Since we are applying the HR method to essentially transient signals, the time intervals will necessarily be short. But more important here is the fact that we want to detect the rapid changes in the distribution of power, and this has limited the length of the time interval to 200 sec, which seems to give a reasonable tradeoff between time resolution and stability. A special problem arises when two otherwise identical waves arrive with different

angles of approach, in which case it has been shown that resolution is not possible regardless of the method employed. However, the fact that the time interval has been divided into two blocks reduces this possibility, since any difference in the time duration of the two waves will benefit the resolution, as indicated previously.

Frequency windowing

This problem should be practically eliminated by the introduction of the prefilters used in this study.

Size of array

Fundamental-mode Rayleigh waves with periods around 40 seconds have wavelengths around 150 km, as compared to 110 km for the diameter of the array. This clearly imposes a severe limitation, but it does not, as thoroughly demonstrated above, exclude the possibility of extracting useful information at this frequency.

Quantization errors

This problem, referring to the wavenumber quantization, has been dealt with in great detail in the Appendix. The problem is simple in the way that the effects of it can be evaluated on a probability basis.

Two different problems, although somewhat entangled in each other, are considered in this paper. The first is an investigation of how the Rayleigh wave detection method due to Capon and Evernden (1971) can be applied to NORSAR. In their analysis, Capon and Evernden used only 40 sec period waves recorded at LASA, which, due the larger diameter of the array (200 km) can be analyzed with about the same resolution as 20 sec period waves at NORSAR. A comparison between the two arrays shows that

the average power of the 40 sec period Rayleigh waves is falling off as a function of time at about the same rate. However, at LASA the scatter in the data seems to be somewhat larger than at NORSAR. Another difference between the two arrays is that while Capon and Evernden could conclude that there was a definite advantage in working with 40 sec period Rayleigh waves at LASA, no such general preference can be made between 40 and 20 sec periods at NORSAR. The various reasons for this are discussed in detail above, and it shall only be stressed here that the conclusions are valid of course only for the general type of events which have been used as a basis for reaching the conclusions. Therefore, if we want to detect an underground nuclear explosion where the energy is concentrated in a narrow band around 16 - 18 sec period, we may have to work in that period range even if the interfering event is much better suppressed at 40 sec period. On the other side, in case of the atmospheric explosion discussed above, the signal-to-interference ratio was clearly much better at periods around 40 sec.

The second problem considered in this paper has been that of multipathing. The various detailed examples given above demonstrate that for practically all events in the teleseismic distance range a severe multipathing of the Rayleigh waves takes place. Since it takes smaller objects and smaller discontinuities to affect smaller wavelengths, this effect is more pronounced for 20 sec than 40 sec period waves. The cause of the multipathing seems to be associated primarily with continental margins. In other cases, specifically around the Arctic ocean where the continental margins may be far out at sea, the reflections and refractions still often seemed to take place near the boundaries of the continents, in which case a mountain barrier or at least a rapid change in elevation must account for the phenomenon.

At other occasions the multipathing could be attributed to mid-continent mountain chains, especially the Himalayas, and also mid-oceanic ridges, notably the mid-Atlantic ridge.

A few other aspects of the multipathing should also be mentioned. First of all, it obviously complicates the detection problem a great deal, and, in case of interfering events, makes it more difficult to determine from which event some energy may be coming. A great help here is the fact that the multipathing is consistent for similar source regions, which makes it appropriate to use reference or master events, as demonstrated above in the case of a nuclear explosion. Another aspect of the problem is the effect on Rayleigh wave magnitude. It has been demonstrated in this paper that at 40 sec period the onset is usually clearly defined, arriving at almost true azimuth, while the picture at 20 sec period is much more complicated. There is often no clear arrival, and the multipathing may be severe already quite early in the records. This means that the observed dispersion may be as much a function of the amount and type of multipathing than of the dispersive characteristics of the medium along the propagation path. The effect that this would have on the magnitude measured through the amplitude of one particular cycle is obvious, pointing towards the preference of an algorithm using the information from a wider band both in time and frequency. Besides this, the multipathing also strongly affects the precision with which one can measure group velocities. Traditionally, group velocity studies have assumed that the energy is ariving along great circle paths, considering only the uncertainty with which the arrival time of any particular frequency could be determined. The results documented in this paper have

demonstrated that the distance which any particular wavelet has travelled may be anything between one and two epicentral distances, and even more if a longer record is studied.

One more aspect of the present detectability problem should be mentioned, namely, the probability with which the Rayleigh waves from one event will interfere with the Rayleigh waves from another event. This probability is obviously quite high, since one large event may affect the records for several hours. It would vary, though, from one station to another depending upon the location with respect to the seismicity zones, and from one time to another with respect to the noise level. An indication of the problem at hand is given in Fig. 24, showing the average noise level of the LPZ sensors at NORSAR over a period of 20 days. Each spike indicates an event, and at other times, when the noise level is lower, the effect is even more dramatic. No effort has been made here to evaluate more accurately the amount of interference at NORSAR, but is is probably not unrealistic to assume that as much as 20% of the well-recorded Rayleigh waves are affected by another event. Besides the fact that this stresses the importance of the present effort to find useful detection methods for Rayleigh waves, it also is an effect which often has been disregarded in analyses of the detection capabilities of stations and networks.

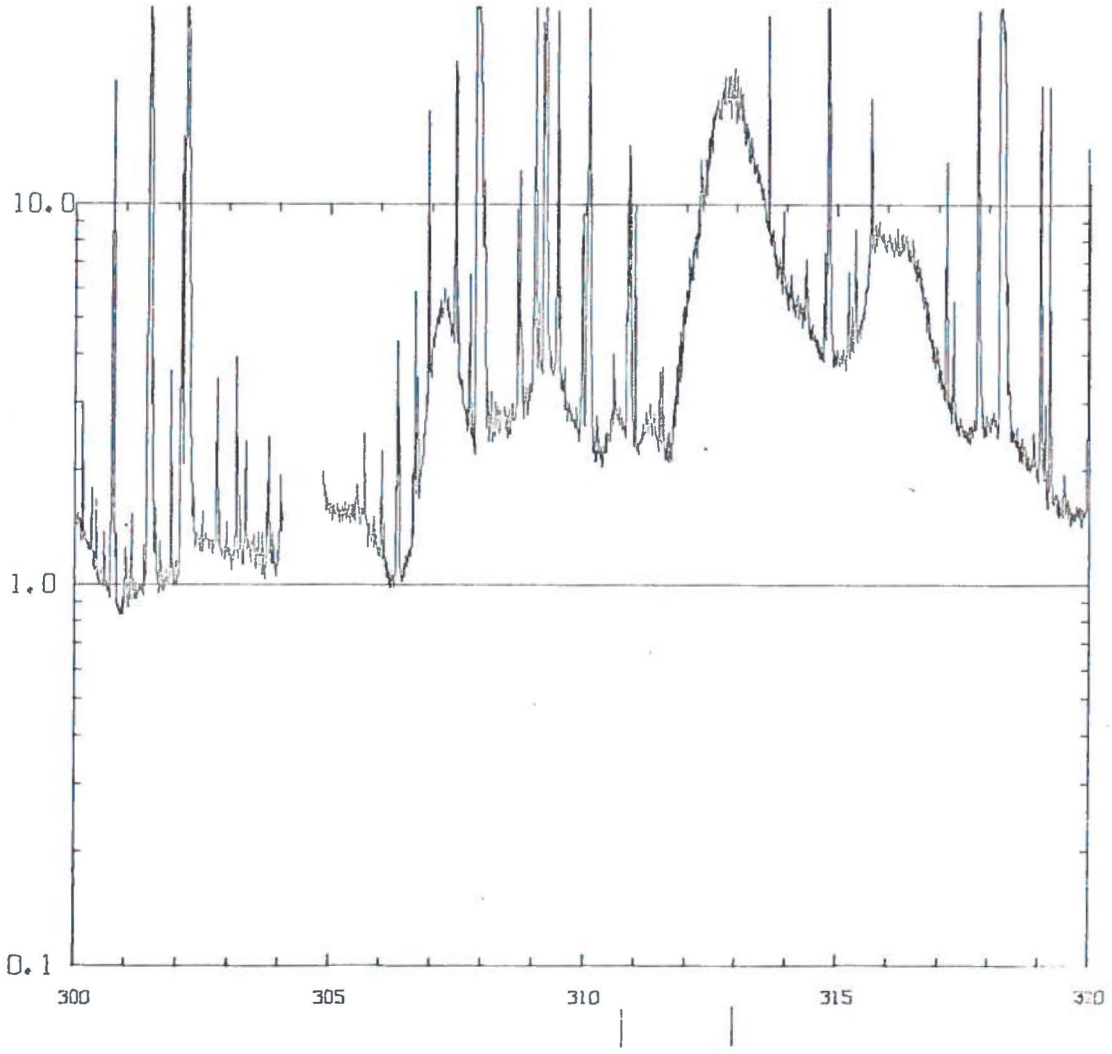

Fig. 24 Average NORSAR long period noise level for days 300-320 in 1972. The curve is calculated through a long term integration process, and sampled every 15 minutes. Each spike indicates an event. The vertical scaling is in relative amplitude. A variation in the level of the background noise by a factor of 30 can be seen, and the peak around day 313 is a typical microseismic storm.

REFERENCES

Bungum, H., and E.S. Husebye (1974): Analysis of the operational capabilities for detection and location of seismic events at NORSAR, Bull. Seism. Soc. Am., in press.

Bungum, H., E.S. Husebye and F. Ringdal (1971): The NORSAR array and preliminary results of data analysis, Geophys. J.R. astr. Soc., Vol 25, 115-126.

Capon, J. (1969): High-resolution frequency-wavenumber spectrum analysis, Proc. IEEE, Vol 57, 1408-1418.

Capon, J. (1970): Analysis of Rayleigh-wave multipath propagation at LASA, Bull. Seism. Soc. Am., Vol 60, 1701-1731.

Capon, J. (1971): Comparison of Love and Rayleigh-wave multipath propagation at LASA, Bull. Seism. Soc. Am., Vol 61, 1327-1344.

Capon, J., and J.F. Evernden (1971): Detection of interfering Rayleigh waves at LASA, Bull. Seism. Soc. Am., Vol 61, 807-849.

Filson, J., and H. Bungum (1972): Initial discrimination results from the Norwegian Seismic Array, Geophys. J.R. astr. Soc., Vol 31, 315-328.

Marshall, P.D., and P.W. Basham (1972): Discrimination between earthquakes and underground explosions employing an improved M_s scale, Geophys. J.R. astr. Soc., Vol 28, 431-458.

Oliver, J. (1962): A summary of observed seismic surface wave dispersion, Bull. Seism. Soc. Am., Vol 52, 81-86.

Smart, E., and E.A. Flinn (1971): Fast frequency-wavenumber analysis and Fisher signal detection in real-time infrasonic array data processing, Geophys. J. R. astr. Soc., Vol 26, 279-284.

APPENDIX

QUANTIZATION ERRORS IN WAVENUMBER SPACE

The high-resolution (HR) frequency-wavenumber analysis is performed in such a way that power estimates are obtained for a number of discrete points in wavenumber (k-) space. These points, as shown in Fig. A1, are distributed in a regular and equi-spaced grid system since this is most efficient when no prior knowledge is assumed about the power distribution. Besides that, a regular grid system is computationally convenient. Then, if no smoothing or interpolation is applied to these grid values, only a limited number of possibilities are available for the estimate of the point of maximum power, which is the sought-after parameter in this study. The k-space quantization error thereby introduced will be dependent upon the density of the grid points, which is always limited by computer time restrictions. It is the purpose of this Appendix to evaluate the size and the distribution of this error, the knowledge of which is essential in the interpretation of the k-space spectra.

Figure A1 shows one quadrant of the k-space grid used in this study. It consists of 21 × 21 equally spaced points, covering a wavenumber distance of ±0.01 c/km in each direction. The frequency here is 0.025 Hz, or 40 sec period. For the frequency 0.050 Hz (20 sec period) the grid size has been ±0.02 c/km with the same number of points, which leads to identical quantization errors for the two frequencies. Since the velocity (v) is related to the frequency (f) and the wavenumber (k) through the formula

$$v = f/k \qquad \text{(A1)}$$

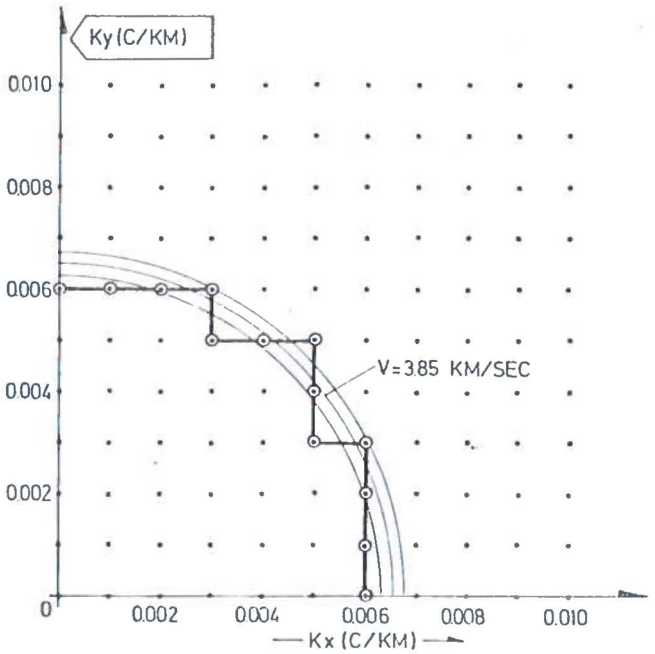

Fig. A1 The wavenumber grid used in this paper for analysis of 40 sec period data. The three circles indicate the expected phase velocity (3.85 km/sec), and the range for the standard deviation. The small circles connected by straight lines are the grid points which are closest to points on this particular phase velocity circle.

where

$$k = (k_x^2 + k_y^2)^{\frac{1}{2}} \qquad \text{(A2)}$$

the constant-velocity locus will be a circle in k-space. This circle is drawn in Fig. A1, for a velocity of 3.85 km/sec, which is used throughout this study as the most probable phase velocity for 40 sec period Rayleigh waves recorded at NORSAR. This is slightly lower than the estimate of continental phase velocities reported by Oliver (1962), and it is also close to the average of the phase velocities observed in this study. Now, for a wave with azimuth anywhere between 0° and 90° and velocity 3.85 km/sec, the HR method using the grid in Fig. A1 has only 13 possible answers, indicated by small circles connected by straight lines. For the velocity, there are only 7 possibilities ranging from 3.5 to 4.3 km/sec. It is also easily seen that the azimuth error may be as large as about 5°.

The example given above requires a single true velocity. That would not be so if the crust and upper mantle under NORSAR have a certain amount of anisotropy, in which case the phase velocities would be azimuthally dependent. An indication to that effect is the fact that the 40 sec period phase velocities for the first time interval vary between 3.4 and 4.1 km/sec (Table 3), and it has been checked that these particular velocities are not seriously affected by quantization errors. The phase velocities for 20 sec period correlate well with those at 40 sec, and the phase velocity is 0.15 km/sec below in average. Therefore, we shall proceed from here assuming that the

true velocity, or wavenumber, is represented by a probability distribution. The natural choice is a Gaussian distribution,

$$p(k) = (2\pi)^{-\frac{1}{2}} \sigma^{-1} \exp[-\tfrac{1}{2}(\frac{k-\bar{k}}{\sigma})^2] \qquad (A3)$$

In the present example, the wavenumber average is $\bar{k}$= 0.025/3.85≈0.0065 c/km, which is also in this case the wavenumber expectation. As for the standard deviation (σ), that is dependent upon the amount of anisotropy of the crust and upper mantle under NORSAR, which is so far not known. However, as an intelligent guess partly based on the observed azimuthal distribution of phase velocities, we have given σ a value of 0.00025 c/km, which corresponds to a velocity range of 3.71 to 4.00 km/sec. This is the velocity range corresponding to the outermost circles in Fig. A1. Standard deviations cannot be given in velocity, since the distribution there is skew due to the non-linear relationship between wavenumber and velocity.

If we are given the distribution of wavenumbers defined above, the distributions of quantization errors in azimuth and phase velocity can now be obtained. This was done numerically by integrating over k-space the product of the quantization error in the point (k_x, k_y) and the probability of occurrence of that particular velocity. For an expected velocity of 3.85 km/sec corresponding to 40 sec period Rayleigh waves, the results are given in Figs. A2 and A3, for azimuth and velocity errors, respectively. The density distribution for azimuth errors is bell-shaped with only 50% of the occurrences within $\pm 2.2^{\circ}$ but with fully 90% within 4.3°. The distribution

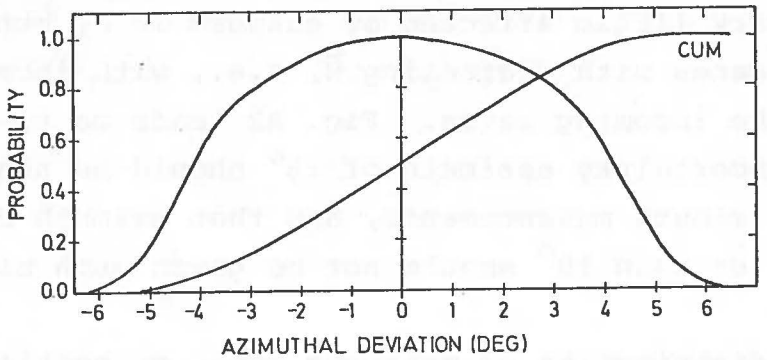

Fig. A2 Normalized incremental and cumulative distributions of azimuthal quantization errors using the wavenumber grid in Fig. A1, and an expected phase velocity of 3.85 km/sec.

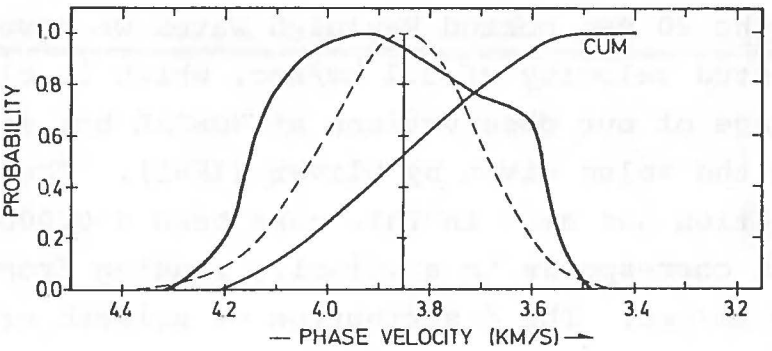

Fig. A3 Normalized incremental and cumulative distributions of measured wave velocities using the wavenumber grid in Fig. A1, and an expected phase velocity of 3.85 km/sec with a distribution as indicated by the dotted line.

is very little affected by changes in σ, but the error increases with decreasing $\bar{k}$, i.e., with increasing velocity of the incoming waves. Fig. A2 leads us to conclude that an uncertainty estimate of $\pm 5^{\circ}$ should be associated to our azimuth measurements, and that azimuth differences smaller than 10° should not be given much significance.

The distribution of measured phase velocities is given in Fig. A3, together with the distribution of expected velocities. The figure shows a fairly skew and oddly-shaped distribution, with almost the same probability over a relatively large velocity range. This leads us to conclude that for the 40 sec period waves we should accept as valid observations any phase velocity in the range 3.5-4.2 km/sec.

For the 20 sec period Rayleigh waves we have assumed an expected velocity of 3.7 km/sec, which is close to the average of our observations at NORSAR but somewhat higher than the value given by Oliver (1962). The standard deviation has also in this case been σ=0.00025 c/km, which corresponds to a velocity ranging from 3.57 to 3.84 km/sec. The distribution of azimuth errors is almost identical with the one in Fig. A2, but the velocity distribution, as shown in Fig. A4, is somewhat different, this time peaking at a lower velocity than the expected. Based on this distribution, the accepted velocity range for 20 sec period waves will be 3.4-4.0 km/sec.

In conclusion, what we have demonstrated in this Appendix is that the azimuth errors due to quantization are in the range $\pm 5^{\circ}$, that the accepted phase velocity range for 40 sec period Rayleigh waves is 3.5-4.2 km/sec, and that the range for 20 sec period waves is 3.4-4.0 km/sec.

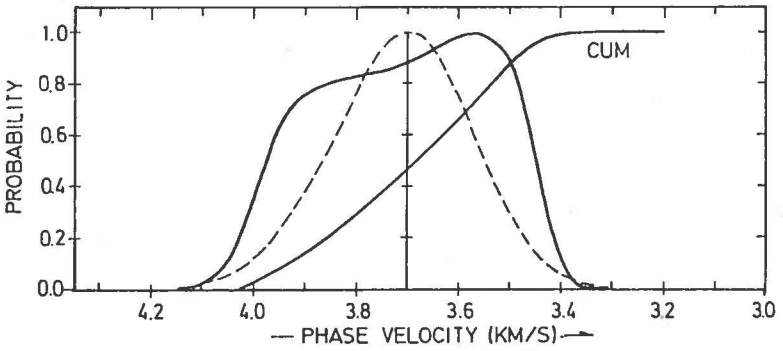

Fig. A4 Normalized incremental and cumulative distributions of measured phase velocities using the wavenumber grid in Fig. A1, and an expected phase velocity of 3.70 km/sec with a distribution as indicated by the dotted line.